performed on days 2–8 after transfection, and then the cells were cultured in normal medium for another 10 days. The vectors and stable transfectant HEK293 cells were designated as pcDNA-mock, pcDNA-GFP, pcDNA-SRPX2/GFP, HEK293-pcDNA-mock, HEK293-pcDNA-GFP and HEK293-pcDNA-SRPX2/GFP.

SRPX2 cDNA in pcDNA3.1 vector was cut out and transferred into a pQCLIN retroviral vector (BD Biosciences Clontech, San Diego, CA) together with enhanced green fluorescent protein (EGFP) following internal ribosome entry site sequence (IRES) to monitor the expression of the inserts indirectly. A pVSV-G vector (Clontech, Palo Alt, CA) for the constitution of the viral envelope and the pQCXIX constructs were cotransfected into the GP2-293 cells using FuGENE6 transfection reagent. Briefly, 80% confluent cells cultured on a 10-cm dish were transfected with 2 μg pVSV-G plus 6 μg pQCXIX vectors. After 48 hr of transfection, the culture medium was collected and the viral particles were concentrated by centrifugation at 15,000g for 3 hr at 4°C. The viral pellet was then resuspended in fresh RPMI1640 medium. The titer of the viral vector was calculated by counting the EGFP-positive cells that were infected by serial dilutions of virus-containing media, and the multiplicity of infection (MOI) was then determined. The viral vector and stable viral transfectant cells in each cell line were designated as pQCLIN-EGFP, pQCLIN-SRPX2, HEK293-pQCLIN-EGFP, HEK293-pQCLIN-SRPX2, MKN1-pQCLIN-EGFP and MKN1-pQCLIN-SRPX2.

Patients and samples

An analysis of SRPX2 expression levels and clinical features was performed using data from patients aged 20 to 75 years and with histologically confirmed, Stage IV gastric cancer. Additional inclusion criteria included an Eastern Cooperative Oncology Group performance status of 0–2. The exclusion criteria included prior chemotherapy or major surgery. Fifty-seven gastric cancer samples were evaluated in this study. All the patients received chemotherapy after registration and endoscopical biopsy. Gastric cancer and noncancerous gastric mucosa samples were evaluated for SRPX2 expression in the first consecutive 24 patients. This study was approved by the institutional review board of the National Cancer Center Hospital, and written informed consent was obtained from all the patients. Endoscopic biopsy samples were immediately placed in an RNA stabilization solution (Isogen; Nippongene, Tokyo, Japan) and stored at −80°C. Other biopsy samples obtained from the same location were reviewed by a pathologist to confirm the presence of tumor cells. The RNA extraction method and the quality check protocol have been previously described.[10]

Real-time reverse-transcription PCR

One microgram of total RNA from normal tissue purchased from Clontech and from a cultured cell line was converted to cDNA using a GeneAmp[R] RNA-PCR kit (Applied Biosystems, CA). Real-time PCR was carried out using the Applied Biosystems 7900HT Fast Real-time PCR System (Applied Biosystems) under the following conditions: 95°C for 6 min, 40 cycles of 95°C for 15 sec and 60°C for 1 min. Glyceraldehyde 3 phosphate dehydrogenase (GAPD, NM_002046) was used to normalize the expression levels in the subsequent quantitative analyses. To amplify the target genes, the following primers were purchased from TaKaRa (Yotsukaichi, Japan): SRPX2-FW, ACT GGA TTT GCG GCA TGT GA; SRPX2-RW, CCA TGT TGA AGT AGG AGC GAG TGA; GAPD-FW, GCA CCG TCA AGG CTG AGA AC; GAPD-RW, ATG GTG GTG AAG ACG CCA GT.

Anti-SRPX2 polyclonal antibody

Rabbit antibodies specific for SRPX2 were obtained by immunizing rabbits with SRPX2 peptide (FIDDYLLSNQELTQ) according to a previously described method,[2] and IgG was purified from serum using standard protocols.

SRPX2-conditioned medium

The media in which subconfluent HEK293-pQCLIN-EGFP, HEK293-pQCLIN-SRPX2, MKN1-pQCLIN-EGFP and MKN1-pQCLIN-SRPX2 cells were being cultured was replaced with a serum-reduced medium (OPTI-MEM; GIBCO), the cells were cultured for an additional 24 hr and the conditioned-media were collected. The media were filtered using Millex-GS (Millipore, Bedford, MA) and concentrated using the Amicon Ultra (Millipore) and stored at −80°C. The concentration of the conditioned-medium was measured using a BCA protein assay (Pierce Biotechnology, Rockford, IL) and equalized.

Western blot analysis

The antibodies used in this study were anti-GFP (Invitrogen, Carlsbad, CA), anti-focal adhesion kinase (anti-FAK), anti-p-FAK (pY397) (BD Biosciences), anti-β-actin (Santa Cruz Biotechnology, Santa Cruz, CA) and anti-p-FAK (pY576/577) (Cell Signaling, Beverly, MA).

A Western blot analysis was performed as described previously (Ref. 10). In brief, subconfluent cells were washed with cold phosphate-buffered saline (PBS) and harvested with Lysis A buffer containing 1%Triton X-100, 20 mM Tris-HCl (pH 7.0), 5 mM EDTA, 50 mM sodium chloride, 10 mM sodium pyrophosphate, 50 mM sodium fluoride, 1 mM sodium orthovanadate and a protease inhibitor mix, complete[TM] (Roche Diagnostics). Whole-cell lysates and culture medium were separated using a 2–15% gradient SDS-PAGE and blotted onto a polyvinylidene fluoride membrane. After blocking with 3% bovine serum albumin in a TBS buffer (pH 8.0) with 0.1% Tween-20, the membrane was probed with primary antibody. After rinsing twice with TBS buffer, the membrane was incubated with horseradish peroxidase-conjugated secondary antibody (Cell Signaling) and washed followed by visualization using an ECL detection system (Amersham) and LAS-3000 (Fujifilm, Tokyo, Japan). The data were quantified by automated densitometry using Multigauge Ver 3.0 (Fujifilm). The experiment was performed in triplicate.

Cellular growth assay

HEK293 transfectant cells were incubated on 96-well plates at a density of 2000/well with 180 μL of culture medium at 37°C in 5% CO₂. After 24, 48 or 72 hr of incubation, 20 μL of MTT [3-(4,5-dimethyl-thiazoyl-2-yl)2,5-diphenyltetrazolium bromide] solution (SIGMA) was added and the cultures were incubated for 4 hr at 37°C. After centrifugation, the culture medium was discarded and the wells were filled with DMSO. The absorbance of the cultures at 562 nm was measured using VERSAmax (Japan Molecular Devices, Tokyo, Japan). The experiment was performed in triplicate.

Cellular adhesion assay

EGFP-conditioned or SRPX2-conditioned media obtained from HEK293-pQCLIN-EGFP, HEK293-pQCLIN-SRPX2, MKN1-pQCLIN-EGFP or MKN1-pQCLIN-SRPX2 cells were adjusted to a concentration of 1 mg/mL and 50 μL were incubated at 4°C overnight on 96-well plates. The conditioned media were aspirated, and the wells were washed twice with PBS. The plates were then used in an adhesion assay as conditioned medium-coated 96-well plates. The cells to be analyzed were added to the wells of conditioned medium-coated plates (2 × 10⁴ cells /well) and incubated at 37°C for 1 hr. When treated with FAK inhibitors (PP2 and Herbimycin A; Calbiochem, San Diego, CA), the cells to be analyzed were incubated for 4 hr. The wells were then washed twice with PBS to remove nonadherent cells. Adherent cells were evaluated using the MTT assay as described above. The average O.D. values of 3 wells were used for a single experiment, and the experiment was performed in triplicate.

Migration assay and chemotaxis assay

Migration assays were performed using the Boyden-chamber methods and polycarbonate membranes with an 8-μm pore size
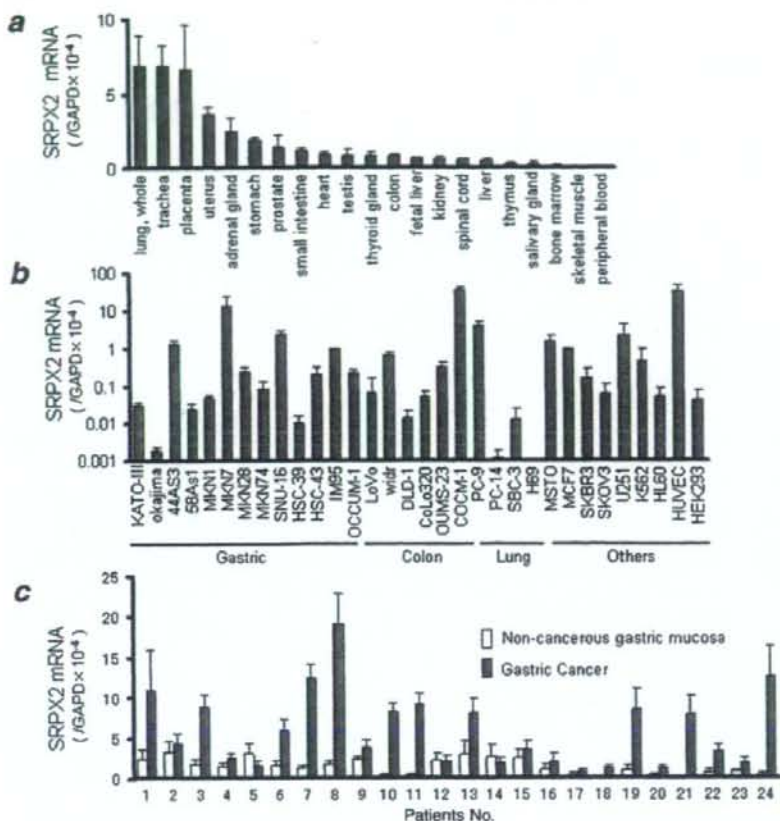
FIGURE 1 – Tissue distribution of *SRPX2* mRNA expression. The mRNA expression levels of *SRPX2* were determined using a real-time RT-PCR analysis in (*a*) human normal tissue; (*b*) 30 human cancer cell lines, HEK293 and HUVEC cell lines and (*c*) paired clinical samples that were endoscopically obtained from gastric cancer and the noncancerous gastric mucosa of the same patients. *GAPD* was used to normalize the expression levels in the subsequent quantitative analyses. The mRNA expression levels of *SRPX2* were significantly higher in the gastric cancer lesions ($p = 0.0004$). Error bars represent the SDs of 3 independent experiments. [Color figure can be viewed in the online issue, which is available at www.interscience.wiley.com.]

(chemotaxicell; KURABO). The membranes were coated with fibronectin on the outer side and dried for 2 hr at room temperature. The cells to be analyzed (2×10^4/well) were then seeded onto the upper chambers with 200 μL of migrating medium (DMEM containing 0.5% FBS), and the upper chambers were placed into the lower chambers of 24-well culture dishes containing 600 μL of DMEM containing 10% FBS. After incubation for 8 hr at 37°C, the media in the upper chambers were aspirated and the nonmigrated cells on the inner sides of the membranes were removed using a cotton swab. The cells that had migrated to the outer side of the membranes were fixed with 4% paraformaldehyde for 10 min and stained with 0.1% crystal violet for 15 min, then counted using a light microscope. The experiment was performed in triplicate.

The chemotaxis assays were performed using SNU-16 cells. A total of 1×10^5 cells were seeded onto the upper chambers with 200 μL of RPMI containing 0.5% FBS. The final concentration at 100 μg/mL of EGFP-conditioned or SRPX2-conditioned medium was added to the 600 μL volume of RPMI1640 containing 0.5% FBS medium in the lower chamber of the 24-well culture dishes. The cells were then incubated for 24 hr at 37°C with 5% CO_2. The number of migrated cells was evaluated as described earlier. The experiment was performed in triplicate.

Wound healing assay

HEK293-pQCLIN-EGFP and HEK293-pQCLIN-SRPX2 cells were plated onto 3.5-cm dishes and incubated in DMEM containing 10% FBS until they reached confluence. Wounds were introduced to the confluent cell monolayer using a plastic pipette tip.

The cells were then cultured with DMEM containing 10% FBS at 37°C. After 4, 8 and 12 hr later, the wound area was photographed using a light microscope and measured. The experiment was performed in triplicate.

Fluorescent microscopy

HEK293-pcDNA-GFP and HEK293-pcDNA-SRPX2/GFP cells were treated with DAPI (6-diamidino-2-phenylindole) to stain the nucleus and photographed using fluorescent microscopy, IX71 (Olympus, Tokyo, Japan).

Statistics

The *t* test was used for comparison between 2 groups and paired *t* test was used for paired-samples in Figure 1*c*. The statistical analysis was performed using Excel software (Microsoft, Redmond, WA). A *p* value < 0.05 was considered significant.

Results

Tissue distribution of SRPX2 mRNA in normal tissues and cell lines

To examine the tissue distribution of *SRPX2* mRNA, we performed real-time RT-PCR for 24 normal human tissues. High expression levels of *SRPX2* mRNA were detected in the placenta, lung, trachea, uterus and adrenal gland, whereas the levels in the peripheral blood, brain and bone marrow were relatively low (Fig. 1*a*). Combined with data from previous reports,[1,2] *SRPX2* mRNA

appears to be widely observed in normal tissues, with particularly high levels detected in the placenta and lung.

SRPX2 expression was also examined in 30 human cancer cell lines, HUVEC and HEK293 cells. A relatively high *SRPX2*

TABLE I – *SRPX2* EXPRESSION AND PATIENT CHARACTERISTICS IN PATIENTS WITH GASTRIC CANCER

Characteristics	Patients No. (%)	SRPX2	
		Expression $(10^{-4}/GAPD)$	p value
Age, years			
≥ 60	31 (54)	12.6 ± 12.5	0.10
<60	26 (46)	11.1 ± 9.1	
Sex			
Male	41 (72)	11.1 ± 9.1	0.61
Female	16 (28)	12.6 ± 12.5	
Histology[1]			
Diff.	22 (39)	11.3 ± 7.9	0.77
Undiff.	32 (56)	12.2 ± 11.7	
Prognosis[2]			
Favorable (≥ 6 months)	37 (65)	9.5 ± 7.2	<0.05
Unfavorable (<6 months)	20 (35)	15.1 ± 13.5	
Total	57		

[1]Histology of endoscopic samples divided into differentiated and undifferentiated type.–[2]Overall survival time from the first day of chemotherapy. A survival time of 6 months was used as the cut-off to divide patients into "Favorable" and "Unfavorable" groups.

mRNA expression level was observed in gastric cancer (44As3, MKN7 and SNU-16), colorectal cancer (WiDr and COCM-1), lung cancer (PC-9), mesothelioma (MSTO), glioma (U251) and HUVEC. These results suggest that a variety of cancer and vascular endothelial cells express *SRPX2* (Fig. 1*b*).

Overexpression of SRPX2 mRNA in gastric cancer tissues

The expression of *SRPX2* mRNA was analyzed for paired tissues of gastric cancer and noncancerous gastric mucosa obtained from 24 gastric cancer patients. A paired *t* test demonstrated that *SRPX2* expression was significantly increased ($p = 0.0004$) in the cancerous tissues, compared to the noncancerous gastric mucosa (Fig. 1*c*). The *SRPX2* mRNA expression levels in the gastric cancer and noncancerous gastric mucosa were 6.6 ± 5.4 and 1.8 ± 1.2 ($\times 10^{-4}/GAPD$), respectively. Although the reason is unclear, 2 groups seemed to be present: 1 group with very high expression levels in cancerous tissues and another group with no difference in the expression levels between cancerous and noncancerous lesions.

To clarify the clinical significance of *SRPX2* expression, we examined the expression in an additional 57 gastric cancer samples using real-time RT-PCR and analyzed the correlations between *SRPX2* expression and clinical characteristics (Table I). Age, sex and histological cancer type were not correlated with *SRPX2* expression. However, patients with an unfavorable outcome, in whom the overall survival time (OS) was less than 6 months, exhibited significantly high expression levels of *SRPX2* in
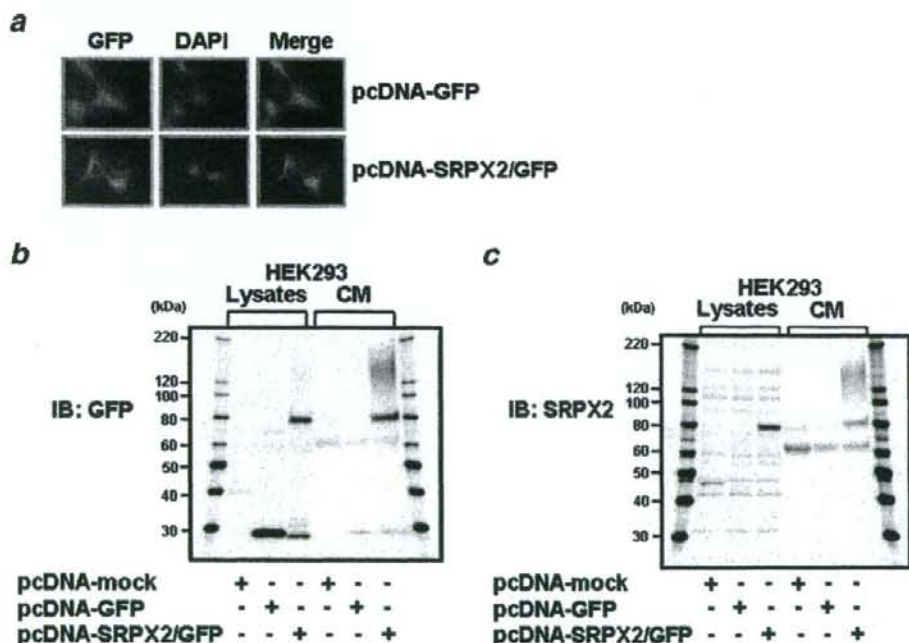

FIGURE 2 – Cellular distribution of SRPX2-GFP fusion protein. To examine the cellular distribution of SRPX2, we created cell lines expressing a fusion protein of SRPX2-GFP. The empty vector, GFP and SRPX2-GFP vectors were transfected into HEK293 cells using FuGENE6 transfection reagent. The vectors and stable transfectant cells in the HEK293 cells were designated as pcDNA-mock, pcDNA-GFP, pcDNA-SRPX2/GFP, HEK293-pcDNA-mock, HEK293-pcDNA-GFP and HEK293-pcDNA-SRPX2/GFP. (*a*) Fluorescence microscopy of HEK293-pcDNA-GFP (upper panel) and pcDNA-SRPX2/GFP cells (lower panel). The SRPX2/GFP fusion protein (green) showed a cytoplasmic distribution. The nucleus was stained by DAPI (blue). Western blot analysis detected by (*b*) anti-GFP antibody and (*c*) anti-SRPX2 antibody for HEK293-pcDNA-mock, HEK293-pcDNA-GFP and HEK293- pcDNA-SRPX2/GFP cells. Both the anti-GFP and the anti-SRPX2 antibodies detected the SRPX2-GFP fusion protein at ~80 kDa in the cell lysate and the secreted form at 150–180 kDa. IB, immunoblot; CM, culture medium.
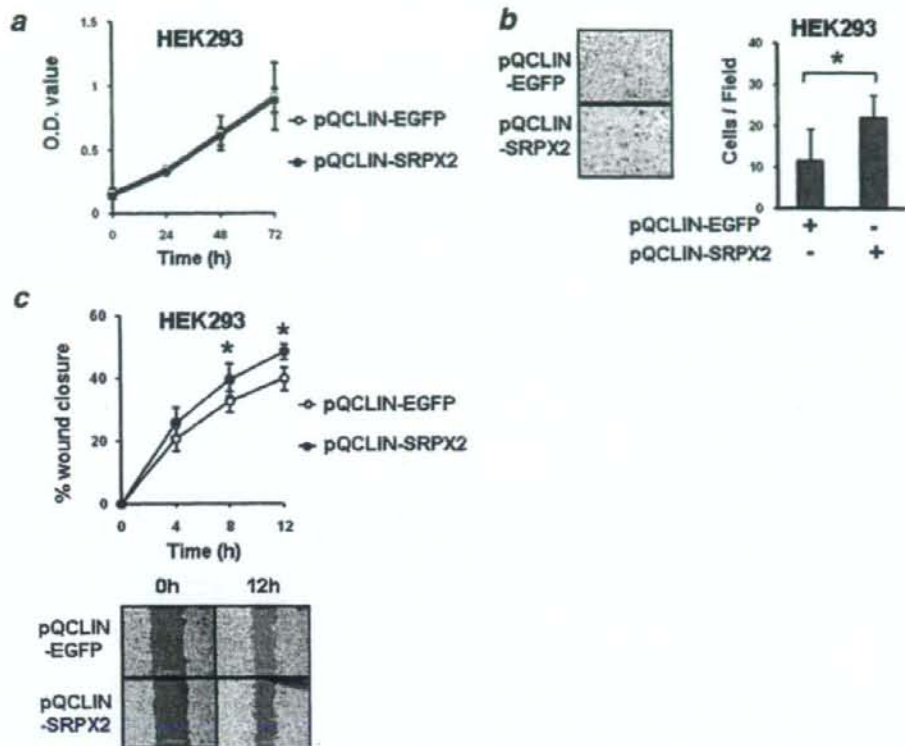
FIGURE 3 – SRPX2-introduced cells enhanced cellular migration but not cellular growth. Viral vectors containing EGFP and SRPX2 were constructed as pQCLIN-EGFP and pQLIN-SRPX2, respectively. These stable cell lines, retrovirally introduced into HEK293 cells, were designated as HEK293-pQCLIN-EGFP and HEK293-pQCLIN-SRPX2, respectively. (*a*) Cellular growth was examined using an MTT assay. No difference in cellular growth was observed between HEK293-pQCLIN-EGFP and HEK293-pQCLIN-SRPX2 cells. (*b*) Migration assay. Cells (2 × 10⁴/well) were seeded into the upper chambers with serum-reduced medium (DMEM with 0.5% FBS). The upper chambers, with fibronectin coated on the outer side of the membrane, were then placed in the lower chambers of a 24-well culture plate containing DMEM with 10% FBS. After incubation for 8 hr at 37°C, medium was aspirated and the nonmigrated cells on the inner side of the membrane were removed using a cotton swab. The migrated cells on the outer side of the membrane were fixed, stained and counted using a light microscope. The experiment was performed in triplicate. The left panels show representative data. (*c*) Wound healing assay for HEK293-pQCLIN-EGFP and HEK293-pQCLIN-SRPX2 cells. Wounds were introduced to the confluent cell monolayer using a plastic pipette tip. After 4, 8 and 12 hr, the wound area was photographed and measured. The lower panels show representative data. The experiment was performed in triplicate. *: $p < 0.05$. EGFP, enhanced green fluorescent protein.

cancerous tissues ($p < 0.05$). The *SRPX2* expression levels in patients with an unfavorable outcome (OS < 6 months) and in those with a favorable outcome (OS > 6 months) were 9.5 ± 7.2 and 15.1 ± 13.5 ($\times 10^{-4}$/*GAPD*), respectively. This result suggests that *SRPX2* might be a prognostic biomarker, that is, associated with a malignant phenotype in gastric cancer.

### SRPX2 is secreted into culture medium and localized in cytoplasm

Because the cellular distribution of an uncharacterized protein often suggest its biological function (*e.g.*, transcription factors tend to be localized in the nucleus), we tried to identify the cellular distribution of SRPX2 using a SRPX2-GFP fusion protein. We introduced an empty vector, GFP, or SRPX2 fused with GFP into HEK293 cells to create the following stable cell lines: HEK293-pcDNA-mock, HEK293-pcDNA-GFP and HEK293- pcDNA-SRPX2/GFP, respectively. The SRPX2-GFP fusion protein exhibited a cytoplasmic distribution (Fig. 2*a*). The protein expression of SRPX2 was then analyzed using western blotting and both anti-GFP and anti-SRPX2 antibodies (Figs. 2*b* and 2*c*). Western blot-

ting with anti-GFP antibody revealed that an SRPX2-GFP fusion protein with a molecular weight (M.W.) of ~80 kDa was detected in both the cell lysates and the culture medium. A similar result was observed using anti-SRPX2 antibody. In addition, an SRPX2/GFP protein with a molecular weight of 150–180 kDa was observed in the culture medium when analyzed using both anti-GFP and anti-SRPX2 antibodies. The SRPX2 protein was detected as 2 bands with molecular weights of ~80 kDa and 150–180 kDa (containing a GFP protein of 30 kDa). The band was consistent with the estimated molecular weight of SRPX2, 53 kDa. The higher band was only observed in the culture medium and was detected using both anti-GFP and anti-SRPX2 antibodies.

SRPX2-introduced cells enhanced cellular migration but not cellular growth

To elucidate the biological function of SRPX2, EGFP or SRPX2 was retrovirally introduced into HEK293 cells. The stable cell lines were designated as HEK293-pQCLIN-EGFP and HEK293-pQCLIN-SRPX2, respectively. We then performed cellular growth assays using these cells (Fig. 3*a*). No difference in
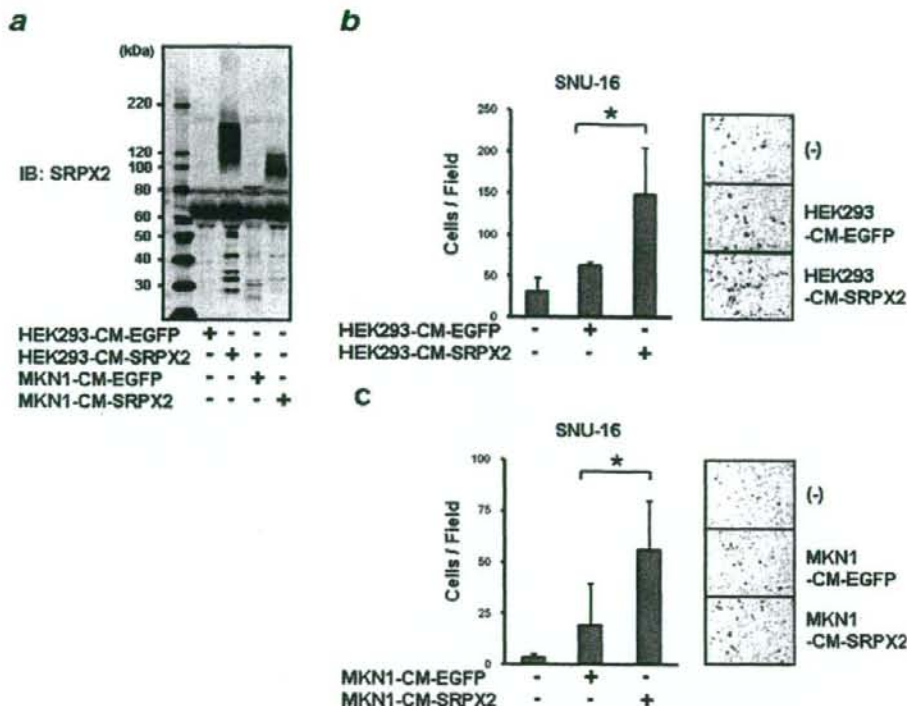
FIGURE 4 – SRPX2-conditioned medium enhanced cellular migration. (a) Western blotting for conditioned medium obtained from the stable cell lines, HEK293-pQCLIN-EGFP, HEK293-pQCLIN-SRPX2, MKN1-pQCLIN-EGFP and MKN1-pQCLIN-SRPX2. Each concentration of conditioned medium was adjusted to 1 mg/mL and diluted before use. Further details are described in the "Material and methods" section. IB, immunoblotting; HEK293-CM-EGFP, conditioned medium from HEK293-pQCLIN-EGFP cells; HEK293-CM-SRPX2, conditioned medium from HEK293-pQCLIN-SRPX2 cells; MKN1-CM-EGFP, conditioned medium from MKN1-pQCLIN-EGFP cells; MKN1-CM-SRPX2, conditioned medium from MKN1-pQCLIN-SRPX2 cells. The role of SRPX2 in cellular migration was assessed in the gastric cancer cell line, SNU-16, using a migration assay and EGFP- or SRPX2-conditioned medium from (b) HEK293-pQCLIN-EGFP or -SRPX2 cells and from (c) MKN1-pQCLIN-EGFP or -SRPX2 cells. A total of 1×10^5 SNU-16 cells were seeded into the upper chambers with 200 μL of RPMI containing 0.5% FBS. The final concentration of 100 μg/mL of EGFP-conditioned or SRPX2-conditioned medium was added to the 600 μL volume of the RPMI1640 containing 0.5% FBS medium in the lower chamber of the 24-well culture dish. The cells were incubated for 24 hr at 37°C. The number of migrated cells was evaluated as described earlier. The experiment was performed in triplicate. Representative data is shown in the right panels. The SRPX2-conditioned medium significantly enhanced cellular motility ($p < 0.05$) by about 2-fold, compared to the EGFP-conditioned medium. Data are shown as the mean ± SD of 3 independent experiments. *: $p < 0.05$.

cellular growth was seen between the cells, indicating that SRPX2 is not involved in cellular growth in HEK293 cells.

We next performed a migration assay to assess the role of SRPX2 in cellular motility. The cellular migration activity of the HEK293-pQCLIN-SRPX2 cells was significantly enhanced, compared to the EGFP transfectant cells ($p = 0.03$, Fig. 3b). A wound healing assay also demonstrated that the cellular motility of HEK293-pQCLIN-SRPX2 cells was significantly enhanced, compared to that of EGFP transfectant cells, at 8 and 12 hr after wound infliction ($p < 0.05$, Fig. 3c). Although the actual difference in the wound healing assay result was relatively small, these results indicate that SRPX2 is involved in cellular motility.

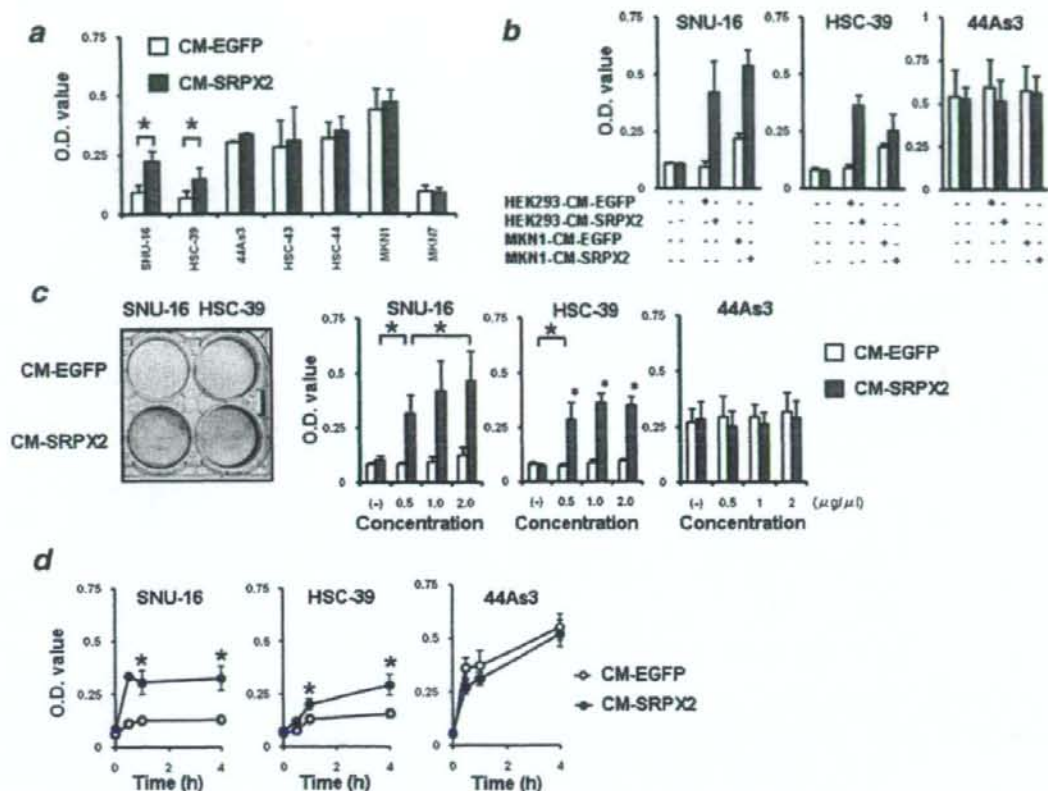*SRPX2-conditioned medium enhanced cellular migration*

EGFP or SRPX2 was also introduced into a gastric cancer cell line, MKN1, and the SRPX2-conditioned media obtained from MKN1 and HEK293 cells were subjected to a migration assay. The transfected cells mainly produced the secreted type of SRPX2 protein with the higher molecular weight, as detected using western blot analysis. The SRPX2 proteins produced by MKN1 and

HEK293 cells were observed at ~95 kDa and 110–150 kDa, respectively (Fig. 4a). This difference in molecular weight might be due to glycosylation.

The role of the secreted SRPX2 protein in the conditioned medium on cellular migration was assessed to SNU-16 cells using a migration assay. SNU-16 cells were incubated for 24 hr in a normal culture medium containing 100 μg/mL of EGFP- or SRPX2-conditioned medium from HEK293-pQCLIN-EGFP or -SRPX2 cells added to the lower chamber of the 24-well culture dish. The SRPX2-conditioned medium significantly enhanced the cellular motility of the SNU-16 cells ($p < 0.05$) by about 2-fold higher than that of the EGFP-conditioned medium (Fig. 4b). Similar results were observed using conditioned medium from MKN1-pQCLIN-EGFP or -SRPX2 cells (Fig. 4c). This result indicates that the secreted SRPX2 protein increased cellular motility in gastric cancer cells.

SRPX2 protein promoted cellular attachment

We examined the cellular adhesion potential of 7 gastric cancer cell lines cultured on EGFP- and SRPX2-conditioned medium-

FIGURE 5 – SRPX2 protein enhanced cellular attachment. EGFP-conditioned or SRPX2-conditioned medium was adjusted to a concentration of 1 mg/mL and 50 μL was placed at 4°C overnight on 96-well plates. The conditioned medium was aspirated, and the wells were washed twice with phosphate-buffered saline (PBS). The plates were used in the adhesion assay as conditioned medium-coated 96-well plates. The cells to be analyzed (2×10^4 cells /well) were seeded into the wells of conditioned medium-coated plates and incubated at 37°C for 1 hr. The wells were then washed twice with PBS to remove nonadherent cells. The adherent cells were evaluated using an MTT assay. (*a*) A cellular adhesion assay was performed using 7 gastric cancer cell lines and conditioned medium-coated plates. The numbers of adhered SNU-16 and HSC-39 cells were significantly larger with the SRPX2-conditioned medium coated-plates ($p < 0.05$). (*b*) A cellular adhesion assay was also performed using conditioned medium-coated plates obtained from MKN1-pQCLIN-EGFP and MKN1-pQCLIN-SRPX2 cells. The numbers of adhered SNU-16 and HSC-39 cells, but not 44As3 cells, were significantly larger. (*c*) A cellular adhesion assay was performed using different concentrations of conditioned medium-coated plates. The 6-well-plate-scale data is shown in the left panel. (*d*) Cellular adhesion assay for time-course analysis. Larger numbers of attached SNU-16 and HSC-39 cells were observed from 0.5 to 4 hr. The increase in cellular attachment induced by the SRPX2 protein emerged after a relatively short time (0.5 hr). The experiment was performed in triplicate. CM-EGFP, conditioned medium from HEK293-pQCLIN-EGFP cells; CM-SRPX2, conditioned medium from HEK293-pQCLIN-SRPX2 cells. [Color figure can be viewed in the online issue, which is available at www.interscience.wiley.com.]

coated plates. Five of the gastric cancer cell lines did not increase cellular attachment to the conditioned medium-coated plate. However, the numbers of attached SNU-16 and HSC-39 cells were significantly increased by more than 2-fold by the presence of SRPX2 protein ($p < 0.05$, Fig. 5*a*).

To exclude nonspecific effects, cellular adhesion assays were also performed using conditioned medium-coated plates obtained from MKN1-pQCLIN-EGFP and MKN1-pQCLIN-SRPX2 cells (Fig. 5*b*). The SNU-16 and HSC-39 cells, but not the 44As3 cells, also exhibited a significantly larger number of adhered cells in the presence of SRPX2 protein obtained from the conditioned-medium of MKN1 cells. Cellular adhesion in these 3 cell lines was examined using 4 different concentrations of conditioned medium-coated plates. Similar results were obtained, and a dose-response effect for the conditioned medium was observed in SNU-16 cells (Fig. 5*c*). Time-course experiments revealed that a larger number of attached SNU-16 and HSC-39 cells were observed after

a short time (0.5 hr) to 4 hr after the start of incubation (Fig. 5*d*). Microscopic examination revealed that most of the adhered cells did not exhibit "cell spreading" and instead resembled "cellular attachment." These results demonstrate that SRPX2 is involved in cellular attachment in SNU-16 and HSC-39 cells.

SRPX2 protein increased phosphorylation levels of FAK

FAK plays a key role in cellular adhesion, and FAK signaling is considered to be a major pathway.[11] To gain insight into the function of SRPX2, the phosphorylation levels of FAK in SNU-16 cells were examined after culturing in a medium to which SRPX2-conditioned medium had been added. Increased phosphorylation levels of FAK (pY397 and pY576/577) were observed in SNU-16 cells in the presence of SRPX2, compared to EGFP, after 1–12 hr of culture (Fig. 6*a*). FAK phosphorylation occurred during an early stage (1 hr) and was consistent with the results for cellular
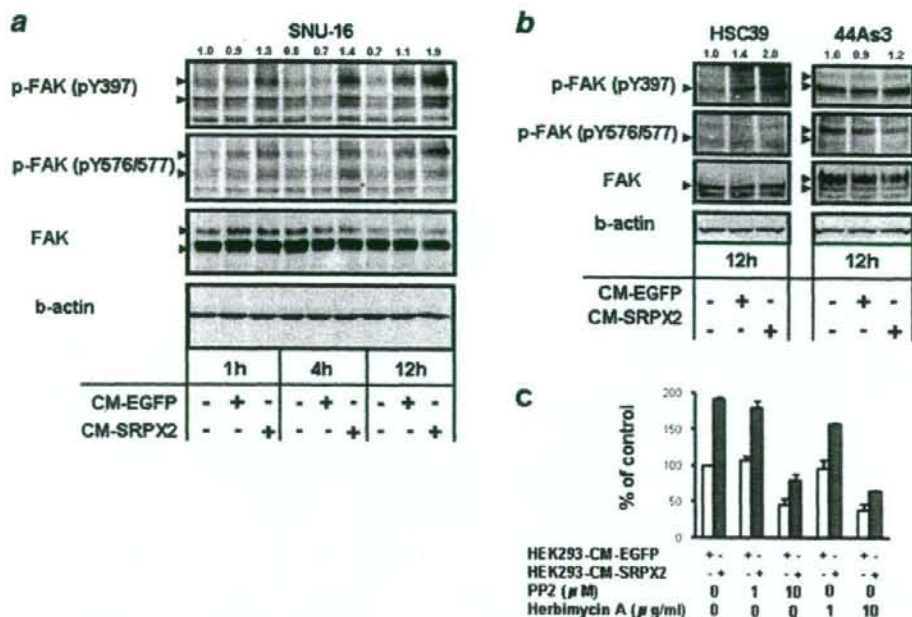
FIGURE 6 – SRPX2 protein increased the phosphorylation levels of FAK. The SNU-16 cells were cultured in RPMI with 0.5% FBS under the presence of GFP or SRPX2-conditioned medium at a final concentration of 100 μg /mL. The cells were collected at 1, 4 and 12 hr after incubation. Ten micrograms of cell lysate were subjected to western blotting using anti-phospho-FAK (pY397 and pY576/577), anti-FAK and anti-β-actin antibodies. A western blot was performed for (a) SNU-16 cells, and (b) HSC-39 and 44As3 cells. FAK, focal adhesion kinase; CM-EGFP, conditioned medium from HEK293-pQCLIN-EGFP cells; CM-SRPX2, conditioned medium from HEK293-pQCLIN-SRPX2 cells. Arrowheads: target molecules. The numerical densitometrical data of phospho-FAK (pY397) is shown above the western blot. (c) SNU-16 cells were treated with FAK inhibitors (PP2; final concentrations 1 or 10 μM and Herbimycin A; final concentrations 1 or 10 μg/mL) in a cellular adhesion assay to assess SRPX2-mediated attachment. Both PP2 and Herbimycin A inhibited cellular attachment of SNU-16 cells in dose-dependent manners. [Color figure can be viewed in the online issue, which is available at www.interscience.wiley.com.]

attachment. FAK phosphorylation by SRPX2 was also stimulated in HSC-39 cells but not in 44As3 cells (Fig. 6b). In addition, to determine whether FAK inhibitors could affect the SPRX2-mediated cellular attachment, the SNU-16 cells were treated with PP2[12] and Herbimycin A[13] to inhibit FAK activity in cellular adhesion assay (Fig. 6c). PP2 and Herbimycin A inhibited cellular attachment of SNU-16 cells in dose-dependent manners.

Although the molecules that transduce the extracellular SRPX2 signal into an intracellular signal remain unknown, these results suggest that the cellular phenotype caused by SRPX2 is associated with the FAK signaling pathway.

Discussion

Considering the structural features of SRPX2, the presence of both the sushi-repeat domain and the HYR domains predict an adhesive function.[4,8] We demonstrated that SRPX2 enhanced cellular motility and cellular attachment, and these findings were consistent with the structural prediction.

The selectin family is the closest family to SRPX2 and SRPX.[3] Selectins are known as cellular adhesion molecules and play key roles in the mediation of early neutrophil rolling on and adherence to endothelial cells.[14] Selectins recognize glycosylated proteins or lipids as their ligands, and this modification is necessary for their interaction.[15] The phylogenetical similarity between SRPX2 and selectins suggests a similar biological function. SNU-16 and HSC-39 cells are basically nonadherent, and the increase in their cellular attachment was a relatively rapid response (0.5 hr). While number of attached cells increased significantly, the attachments

were weak and the cells did not spread on the plates. Thus, the increased cellular attachment induced by SRPX2 seems to resemble neutrophil rolling.

Because the DGEA motif is a potential integrin-binding motif[16] and this motif exists in the first sushi domain of SRPX2, we hypothesized that this motif is a critical binding site for SRPX2's ability to enhance cellular migration and attachment. We examined the inhibitory effect of the DGEA peptide[16] on cell migration and attachment, but no inhibitory effect was observed (data not shown). This result suggests that the cell migration and attachment induced by SRPX2 might be independent of DGEA sequence-mediated signal transduction, or such a sequon does not function in SRPX2.

FAK is a major focal adhesion-associated protein that transmits signals downstream of integrins. FAK signals control important biological events, including cell migration, proliferation and survival, through downstream molecules like Rho, Rac, Rap1, CDC42 and PAK.[11,17,18] Our results demonstrated that SRPX2 protein increased the phosphorylation levels of FAK in SNU-16 and HSC-39 cells, but not in 44As3 cells (Figs. 6a and 6b), and enhanced the cellular adhesive potential in SNU-16 and HSC-39 cells but not in 5 other cell lines (Fig. 5a). We speculate that certain molecules overexpressed in SNU-16 and HSC-39 cells may localize on the cell surface and bind to SRPX2 protein, activating FAK signaling. Recently, Royer-Zemmour et al.[19] demonstrated the interaction of SRPX2 with uPAR (plasminogen activator, uro-kinase receptor) as well as with other partners such as cathepsin B. Because uPAR particularly plays an important and well-known role in various tumoral processes including cell proliferation, migration, invasion and adhesion, and because uPAR-associated

intracellular signaling may act through FAK. The SRPX2/uPAR interaction might provide a possible molecular explanation for the role of SRPX2 in cancer.

Regarding the higher fuzzy smeared-band observed in only the culture medium (Figs. 2b, 2c and 4a), the size of the bands differed considerably between HEK293 and MKN1 cells (110–150 kDa and ~95 kDa, respectively). These results suggest that the higher smeared bands are probably not dimmers, but they may represent a highly glycosylated protein modification. We tried to cut off the N-glycans using N-glycosidase F, but the 150-kDa smeared band did not disappear. We plan to perform additional experiments to clarify the cause of the smeared band in future studies, the results of which will undoubtedly be useful in predicting the function of SRPX2.

Many studies have indicated that selectins, the family most similar to SRPX and SRPX2 proteins, increase the interaction between tumor cells and endothelial cells, leading to tumor progression and metastasis.[20,21] Thus selectins are considered promalignancy factors.[20] Recent reports have shown that selectins positively promote angiogenesis.[22,23] Because HUVEC cells express high levels of SRPX2 mRNA, the involvement of SRPX2 in angiogenesis should be clarified.

In this study, we demonstrated that SRPX2 is overexpressed in gastric cancer, compared to noncancerous gastric mucosa from the same patients, at the transcriptional level. A real-time RT-PCR analysis of 32 cell lines revealed that other cancer cells also express high levels of SRPX2 mRNA. SRPX2 was also overexpressed by more than 10-fold in clinical samples of colorectal cancers, compared to paired colonic mucosa (unpublished data). Thus, SRPX2 overexpression in cancer tissue may not be restricted to gastric cancers. We plan to further examine SRPX2 expression using immunohistochemistry in clinical samples of other cancers in the future.

Although the meaning of SRPX2 overexpression in gastric cancer is unclear, a real-time RT-PCR analysis of clinical samples showed that SRPX2 expression is associated with a poor prognosis in patients with gastric cancer. SRPX2 was first identified as a downstream molecule of E2F-HLF in pro-B acute leukemia with t(17;19) (q23;p13) and has since been reported to contribute to malignant phenotypes.[1] E2F-HLF-positive leukemia is characterized by a poor outcome with bone invasion, hypercalcemia and intravascular coagulation.[24] The clinical features of leukemia and our results for gastric cancer suggest that the biological function of SRPX2 is concerned with oncogenic activity. Further investigations of clinical outcome in relation to SRPX2 expression are needed.

In conclusion, we found that SRPX2 is overexpressed in gastric cancer and plays roles in cellular migration and adhesion in cancer cells. These results provide novel insight into the biological function of SRPX2 in cancer cells.

References

1. Kurosawa H, Goi K, Inukai T, Inaba T, Chang KS, Shinjyo T, Rakestraw KM, Naeve CW, Look AT. Two candidate downstream target genes for E2A-HLF. Blood 1999;93:321–32.
2. Roll P, Rudolf G, Pereira S, Royer B, Scheffer IE, Massacrier A, Valenti MP, Roeckel-Trevisiol N, Jamali S, Beclin C, Seegmuller C, Metz-Lutz MN, et al. SRPX2 mutations in disorders of language cortex and cognition. Hum Mol Genet 2006;15:1195–207.
3. Royer B, Soares DC, Barlow PN, Bontrop RE, Roll P, Robaglia-Schlupp A, Blancher A, Levasseur A, Cau P, Pontarotti P, Szepetowski P. Molecular evolution of the human SRPX2 gene that causes brain disorders of the Rolandic and Sylvian speech areas. BMC Genet 2007;8:72.
4. O'Leary JM, Bromek K, Black GM, Uhrinova S, Schmitz C, Wang X, Krych M, Atkinson JP, Uhrin D, Barlow PN. Backbone dynamics of complement control protein (CCP) modules reveals mobility in binding surfaces. Protein Sci 2004;13:1238–50.
5. Soares DC, Gerloff DL, Syme NR, Coulson AF, Parkinson J, Barlow PN. Large-scale modelling as a route to multiple surface comparisons of the CCP module family. Protein Eng Des Sel 2005;18:379–88.
6. Meindl A, Carvalho MR, Herrmann K, Lorenz B, Achatz H, Apfelstedt-Sylla E, Wittwer B, Ross M, Meitinger T. A gene (SRPX) encoding a sushi-repeat-containing protein is deleted in patients with X-linked retinitis pigmentosa. Hum Mol Genet 1995;4:2339–46.
7. Dry KL, Aldred MA, Edgar AJ, Brown J, Manson FD, Ho MF, Prosser J, Hardwick LJ, Lennon AA, Thomson K, Keuren MV, Kumit DM, et al. Identification of a novel gene, ETX1 from Xp21.1, a candidate gene for X-linked retintis pigmentosa (RP3). Hum Mol Genet 1995;4:2347–53.
8. Callebaut I, Gilges D, Vigon I, Mornon JP. HYR, an extracellular module involved in cellular adhesion and related to the immunoglobulin-like fold. Protein Sci 2000;9:1382–90.
9. Yamada Y, Arao T, Gotoda T, Taniguchi H, Oda I, Shirao K, Shimada Y, Hamaguchi T, Kato K, Hamano T, Koizumi F, Tamura T, et al. Identification of prognostic biomarkers in gastric cancer using endoscopic biopsy samples. Cancer Sci 2008;99:2193–99.
10. Yamanaka R, Arao T, Yajima N, Tsuchiya N, Homma J, Tanaka R, Sano M, Oide A, Sekijima M, Nishio K. Identification of expressed genes characterizing long-term survival in malignant glioma patients. Oncogene 2006;25:5994–6002.
11. Parsons JT. Focal adhesion kinase: the first ten years. J Cell Sci 2003; 116:1409–16.
12. Pala D, Kapoor M, Woods A, Kennedy L, Liu S, Chen S, Bursell L, Lyons KM, Carter DE, Beier F, Leask A. Focal adhesion kinase/Src suppresses early chondrogenesis: central role of CCN2. J Biol Chem 2008;283:9239–47.
13. Lan CC, Wu CS, Chiou MH, Hsieh PC, Yu HS. Low-energy helium-neon laser induces locomotion of the immature melanoblasts and promotes melanogenesis of the more differentiated melanoblasts: recapitulation of vitiligo repigmentation in vitro. J Invest Dermatol 2006; 126:2119–26.
14. Mousa SA. Cell adhesion molecules: potential therapeutic & diagnostic implications. Mol Biotechnol 2008;38:33–40.
15. Vestweber D, Blanks JE. Mechanisms that regulate the function of the selectins and their ligands. Physiol Rev 1999;79:181–213.
16. Mineur P, Guignandon A, Lambert ChA, Amblard M, Lapiere ChM, Nusgens BV. RGDS and DGEA-induced [Ca2+]i signalling in human dermal fibroblasts. Biochim Biophys Acta 2005;1746:28–37.
17. Schaller MD. FAK and paxillin: regulators of N-cadherin adhesion and inhibitors of cell migration? J Cell Biol 2004;166:157–9.
18. Mitra SK, Schlaepfer DD. Integrin-regulated FAK-Src signaling in normal and cancer cells. Curr Opin Cell Biol 2006;18:516–23.
19. Royer-Zemmour B, Ponsole-Lenfant M, Gara H, Roll P, Leveque C, Massacrier A, Ferracci G, Cillario J, Robaglia-Schlupp A, Vincentelli R, Cau P, Szepetowski P. Epileptic and developmental disorders of the speech cortex: ligand/receptor interaction of wild-type and mutant SRPX2 with the plasminogen activator receptor uPAR. Hum Mol Genet 2008;17:3617–30.
20. Witz IP. The selectin-selectin ligand axis in tumor progression. Cancer Metastasis Rev 2008;27:19–30.
21. Barthel SR, Gavino JD, Descheny L, Dimitroff CJ. Targeting selectins and selectin ligands in inflammation and cancer. Expert Opin Ther Targets 2007;11:1473–91.
22. Oh IY, Yoon CH, Hur J, Kim JH, Kim TY, Lee CS, Park KW, Chae IH, Oh BH, Park YB, Kim HS. Involvement of E-selectin in recruitment of endothelial progenitor cells and angiogenesis in ischemic muscle. Blood 2007;110:3891–9.
23. Egami K, Murohara T, Aoki M, Matsuishi T. Ischemia-induced angiogenesis: role of inflammatory response mediated by P-selectin. J Leukoc Biol 2006;79:971–6.
24. Hunger SP. Chromosomal translocations involving the E2A gene in acute lymphoblastic leukemia: clinical features and molecular pathogenesis. Blood 1996;87:1211–24.

A Randomized, Double-Blind, Phase IIa Dose-Finding Study of Vandetanib (ZD6474) in Japanese Patients With Non-Small Cell Lung Cancer

Katsuyuki Kiura, MD, PhD,* Kazuhiko Nakagawa, MD, PhD,†
Tetsu Shinkai, MD, PhD,‡ Kenji Eguchi, MD, PhD,§ Yuichiro Ohe, MD, PhD,‖
Nobuyuki Yamamoto, MD, PhD,¶ Masahiro Tsuboi, MD, PhD,# Soichiro Yokota, MD, PhD,**
Takashi Seto, MD, PhD,†† Haiyi Jiang, MD,‡‡ Kazuto Nishio, MD, PhD,† Nagahiro Saijo, MD, PhD,§
and Masahiro Fukuoka, MD, PhD†

Introduction: Vandetanib (ZACTIMA™) is a once-daily, oral anticancer drug that selectively inhibits vascular endothelial growth factor receptor (VEGFR) and epidermal growth factor receptor (EGFR) signaling. Vandetanib was evaluated as a monotherapy in a randomized, double-blind, dose-finding study in Japan.

Patients and Methods: Eligible patients with locally advanced or metastatic (stage IIIB/IV) or recurrent non-small cell lung cancer, previously treated with chemotherapy, were randomized to receive once-daily oral vandetanib 100, 200, or 300 mg (1:1:1). The primary objective was to determine the objective response rate for each vandetanib dose.

Results: Fifty-three patients received vandetanib (100 mg, $n = 17$; 200 mg, $n = 18$; 300 mg, $n = 18$). The objective response rate in each dose arm was 17.6% (3 of 17; 100 mg), 5.6% (1 of 18; 200 mg), and 16.7% (3 of 18; 300 mg). Common adverse events included rash, diarrhea, hypertension, and asymptomatic QTc prolongation. The adverse event profile was generally consistent with that reported previously for agents that inhibit the VEGFR or EGFR signaling pathways. Among the three responders evaluated for *EGFR* mutation, two had no mutation, and in one case, the *EGFR* mutation status could not be determined by direct DNA sequencing and amplification refractory mutation system assay of *EGFR* exons 19–21. Baseline plasma VEGF levels appeared to be lower in patients who experienced clinical benefit after vandetanib treatment.

Conclusion: In Japanese patients with advanced non-small cell lung cancer, vandetanib monotherapy (100–300 mg/d) demonstrated antitumor activity with an acceptable safety and tolerability profile.

Key Words: Non-small cell lung cancer, Vandetanib, EGFR, VEGFR.

(J Thorac Oncol. 2008;3: 386–393)

Non-small cell lung cancer (NSCLC) accounts for approximately 75% of lung cancers and is the leading cause of cancer-related death worldwide.[1] Despite the introduction of more effective chemotherapeutic agents, new approaches are required to further improve patient outcome and survival. A major focus of new anticancer research is the targeting of cell-signaling pathways that contribute to tumor growth and progression.

Vascular endothelial growth factor receptor (VEGFR) and epidermal growth factor receptor (EGFR) are key drivers of tumor angiogenesis and cell proliferation, respectively, and both pathways have been validated as clinically relevant targets in NSCLC. The addition of bevacizumab, a humanized anti-VEGF-A monoclonal antibody, to paclitaxel and carboplatin has demonstrated clinical benefit in patients with NSCLC,[2] and the EGFR inhibitors gefitinib and erlotinib have demonstrated clinical activity as single agents in NSCLC.[3,4] Furthermore, EGFR is known to regulate the production of VEGF and other proangiogenic factors[5] and resistance to EGFR inhibition has been associated with increased expression of VEGF in a human tumor xenograft model of NSCLC.[6] Therefore, targeting the VEGFR and EGFR pathways may be more effective than inhibiting either pathway alone. This hypothesis is supported by the promising results from early clinical evaluation of erlotinib and bevacizumab in combination in patients with recurrent NSCLC.[7]

Vandetanib (ZACTIMA™) is a once-daily, orally available anticancer drug that inhibits VEGFR- and EGFR-dependent signaling,[8] as well as the RET (REarranged during

*Okayama Graduate School of Medicine, Dentistry, and Pharmaceutical Sciences and Okayama University Hospital, Okayama, Japan; †Kinki University School of Medicine, Osaka, Japan; ‡Shikoku Cancer Center, Ehime, Japan; §Tokai University Hospital, Kanagawa, Japan; ‖National Cancer Center Hospital, Tokyo, Japan; ¶Shizuoka Cancer Center, Shizuoka, Japan; #Tokyo Medical University Hospital, Tokyo, Japan; **Toneyama National Hospital, Osaka, Japan; ††Kyushu Cancer Center, Fukuoka, Japan; ‡‡AstraZeneca KK, Osaka, Japan; and the §§National Cancer Center Hospital East, Chiba, Japan.

Transfection) receptor tyrosine kinase, which is an important growth driver in certain types of thyroid cancer.[9] Early clinical evaluation of vandetanib has demonstrated a promising efficacy and safety profile in a broad population of patients with advanced cancer. Phase I studies in advanced solid tumors conducted in the USA/Australia[10] and Japan[11] showed that once-daily doses of vandetanib (up to and including 300 mg) were generally well tolerated. In the Japanese study, objective tumor responses were observed in 4 of 9 patients with refractory NSCLC. Subsequent phase II studies in advanced NSCLC demonstrated antitumor activity both as a monotherapy and in combination with certain chemotherapy.[12–14] The positive outcome of these phase II trials led to the ongoing phase III evaluation of vandetanib in previously treated advanced NSCLC.

The primary objective of this randomized phase IIa study was to assess the objective response rate (ORR) to vandetanib (100, 200, or 300 mg/d) in Japanese patients with refractory NSCLC. The three doses investigated were selected based on the outcome of the Japanese phase I trial.[11]

PATIENTS AND METHODS

Patients

Patients with histologic or cytologic confirmation of locally advanced/metastatic (stage IIIB/IV) or recurrent NSCLC after failure of 1 or 2 platinum-based chemotherapy regimens were recruited from eight centers in Japan. The main eligibility criteria were age ≥20 years, a WHO performance status of 0 to 2, an estimated life expectancy ≥12 weeks, and completion of prior chemotherapy and/or radiotherapy at least 4 weeks before study entry (8 weeks for chest radiation and 6 weeks for mitomycin C). Patients with squamous cell histology were also eligible, and brain metastases were permitted if patients were asymptomatic and did not require corticosteroid treatment. Key exclusion criteria were a mixed small-cell and non-small cell histology, evidence of severe or uncontrolled systemic diseases, poorly controlled hypertension, a QTc interval ≥460 milliseconds by electrocardiogram during the screening period, and prior treatment with EGFR or VEGFR signaling inhibitors. All patients provided written informed consent. The study was conducted in accordance with the ethical principles stated in the Declaration of Helsinki, applicable guidelines on good clinical practice, local Institutional Review Board approval, and the AstraZeneca policy on Bioethics.

Study Design and Treatments

This was a randomized, double-blind, parallel-group, phase IIa dose-finding multicenter study to assess the efficacy and safety of vandetanib. A total of 53 patients were randomized (1:1:1) to receive once-daily oral vandetanib (100, 200, or 300 mg/d; Figure 1). Patients were stratified by histology (adenocarcinoma versus others), gender (male versus female), and smoking history (smoker versus nonsmoker). Treatment continued until a withdrawal or dose-interruption criterion was met. These criteria included progressive disease (PD), unacceptable toxicity, protocol noncompliance, or voluntary discontinuation by the patient.
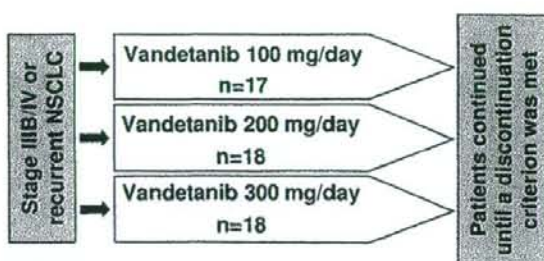

FIGURE 1.   Study design.

Efficacy

The primary objective of the study was to determine ORR with vandetanib monotherapy, using the Response Evaluation Criteria in Solid Tumors (RECIST); assessments were performed at baseline and every 4 weeks for the first 24 weeks of treatment, and then every 8 weeks until withdrawal. A confirmed complete response or partial response (PR) was considered to be an objective tumor response. Investigator assessment of best overall tumor response was used for the primary analysis and these assessments were subsequently submitted to AstraZeneca for review by the response evaluation committee. Secondary efficacy endpoints included time to progression (TTP), duration of response (the time interval between the date of first documented objective tumor response until the date of PD or death), and disease control rate (DCR) for each dose of vandetanib. Time to progression was calculated from the date of randomization until the date of PD or death (in the absence of progression) and estimated using the Kaplan–Meier method. DCR was defined as confirmed complete response, PR, or stable disease (SD) ≥8 weeks.

Safety and Tolerability

Safety was assessed by monitoring for adverse events (AEs) and collecting laboratory data. All AEs were collected for up to 30 days after the last dose of vandetanib and were graded according to Common Terminology Criteria for Adverse Events (CTCAE, version 3). Unless otherwise clinically indicated, 12-lead electrocardiograms were performed twice at screening, weekly for the first 8 weeks of treatment, and then once every 4 weeks thereafter. Vandetanib treatment was interrupted following: a single QTc measurement ≥550 milliseconds; 2 consecutive QTc measurements ≥500 milliseconds but <550 milliseconds; an increase of ≥100 milliseconds from baseline; or an increase of ≥60 milliseconds from baseline QTc to a QTc value ≥460 milliseconds. Upon resolution of QTc prolongation, vandetanib treatment was recommenced at a reduced dose.

Pharmacokinetics

To investigate the pharmacokinetic (PK) profile of vandetanib, blood samples were collected on the same days as scheduled electrocardiogram measurements. Plasma concentrations of vandetanib were determined using reversed-phase liquid chromatography–mass spectrometry. The col-

lected data were related to a nonlinear mixed effects model to estimate population PK using NONMEM V (v 1.1).

Tumor Biomarkers

An exploratory objective of this study was to investigate how variations in copy number or mutational status of the *EGFR* gene affect tumor response in advanced NSCLC patients receiving vandetanib treatment. Tumor biopsy samples were obtained from consenting patients, formalin-fixed, and embedded in paraffin. Gene copy number was investigated by fluorescence in situ hybridization using the LSI EGFR SpectrumOrange/CEP 7 SpectrumGreen probe (Vysis, Abbott Laboratories, IL) according to a previously published method.[15] Tumor samples had a high *EGFR* gene copy number if there was high gene polysomy (≥4 *EGFR* gene copies in ≥40% of tumor cells) or gene amplification (presence of tight *EGFR* gene clusters, an *EGFR* gene to chromosome 7 ratio of ≥2, or ≥15 copies of the *EGFR* gene per tumor cell in ≥10% of analyzed cells).

EGFR mutations were analyzed by DNA sequencing of exons 19–21, and additionally by using the amplification refractory mutation system (ARMS) assay to detect the exon 21 L858R point mutation and the most common exon 19 deletion (del G2235–A2249).[16]

Plasma Biomarkers

Plasma samples were collected from patients at baseline, day 29, and day 57, and stored at $-70°C$. The concentrations of the following angiogenic markers were determined by colorimetric Sandwich ELISA (R&D Systems, Minneapolis, USA): VEGF (Cat. #DVE00), the soluble angiopoietin receptor Tie-2 (Cat. #DTE200), and VEGFR-2 (Cat. #DVR200).

RESULTS

Patient Characteristics

Fifty-three patients were recruited from eight centers in Japan between December 27, 2004, and September 30, 2005. All were randomized on this study and received study drug. Patient characteristics and baseline demographics were generally similar in the three arms, and the patient populations were considered to be appropriate for the dose-finding objectives of this study (Table 1). At the time of data cut-off (23 January 2006), 11 patients were ongoing; PD was the most common reason for discontinuation ($n = 35$). Other reasons for discontinuation were AEs ($n = 6$) and withdrawal of consent ($n = 1$).

Efficacy

The overall ORR was 13.2% (95% CI: 5.5–25.3%) (7 of 53 patients), and all 7 responders were PRs (Table 2). According to vandetanib dose received, the ORRs were 17.6% (95% CI: 3.8–43.4%) (3 of 17 patients; 100 mg), 5.6% (95% CI: 0.1–27.3%) (1 of 18 patients; 200 mg), and 16.7% (95% CI:3.6–41.4%) (3 of 18 patients; 300 mg). In all cases, the response evaluation committee assessment of tumor responses was similar to the investigator assessments. The characteristics of those patients who achieved a PR are described in Table 3. Secondary efficacy assessments are presented in Table 2 and Figure 2.

Safety

Overall, the most common AEs were rash, diarrhea, hypertension, and QTc prolongation (Table 4). In general, no major differences were observed in the incidences of

TABLE 1. Patient Demographic and Baseline Characteristics (Full Analysis Set)

	Vandetanib 100 mg/d ($n = 17$)	Vandetanib 200 mg/d ($n = 18$)	Vandetanib 300 mg/d ($n = 18$)	Total ($n = 53$)
Median age, yr (range)	58 (30–78)	61 (43–77)	61 (44–77)	60 (30–78)
Male (%)	11 (64.7)	12 (66.7)	11 (61.1)	34 (64.2)
Female (%)	6 (35.3)	6 (33.3)	7 (38.9)	19 (35.8)
Smoking history[a]				
No (%)	5 (29.4)	8 (44.4)	7 (38.9)	20 (37.7)
Yes (%)	12 (70.6)	10 (55.6)	11 (61.1)	33 (62.3)
WHO performance status 0/1/2	5/12/0	7/11/0	6/12/0	18/35/0
Previous chemotherapy				
One regimen (%)	13 (76.5)	9 (50.0)	14 (77.8)	36 (67.9)
Two regimens (%)	4 (23.5)	9 (50.0)	4 (22.2)	17 (32.1)
Staging (%)				
IIIB	2 (11.8)	3 (16.7)	1 (5.6)	6 (11.3)
IV	14 (82.4)	12 (66.7)	15 (83.3)	41 (77.4)
Recurrent	1 (5.9)	3 (16.7)	2 (11.1)	6 (11.3)
Histology (%)				
Squamous	5 (29.4)	6 (33.3)	4 (22.2)	15 (28.3)
Adenocarcinoma	11 (64.7)	12 (66.7)	12 (66.7)	35 (66.0)
Other	1 (5.9)	0	2 (11.1)	3 (5.7)
Brain metastasis at study entry (%)	4 (23.5)	3 (16.7)	5 (27.8)	12 (23.6)

[a] No, patients who have smoked <100 cigarettes in their lifetime; Yes, patients who have smoked >100 cigarettes in their lifetime.

TABLE 2. Efficacy Summary

	Vandetanib 100 mg/d (n = 17)	Vandetanib 200 mg/d (n = 18)	Vandetanib 300 mg/d (n = 18)
Primary efficacy assessment			
Best response (RECIST)			
Partial response, n (%)	3 (17.6)	1 (5.6)	3 (16.7)
Stable disease ≥8 wk, n (%)	5 (29.4)	6 (33.3)	8 (44.4)
Disease progression, n (%)	9 (52.9)	10 (55.6)	7 (38.9)
Not evaluable, n (%)	0	1 (5.6)	0
Secondary efficacy assessments			
Disease control ≥8 wk, n (%)	8 (47.1)	7 (38.9)	11 (61.1)
Duration of response (wk)			
Median (range)[a,b]	na	na	15.9 (7.3–20.1)
Time to progression (wk)			
Median (range)[a]	8.3 (4.0–40.7)	12.3 (0–40.3)	12.3 (1.4–32.7)
No. of events	12	13	13

na, not applicable; RECIST, Response Evaluation Criteria in Solid Tumors.
[a] Median estimated using the Kaplan–Meier method.
[b] This parameter could not be estimated in the 100 and 200 mg/d arms owing to the lack of progressions by the date of data cut-off.

TABLE 3. Characteristics of Patients Who Were Partial Responders

Treatment (initial dose)	Gender	Age (yr)	Smoking History[a]	Histology	Previous Chemotherapy Regimens	Time to PR (d)	Duration of Response (d)
100 mg	Male	65	Yes	Adenocarcinoma	1	28	204[b]
100 mg	Female	72	No	Adenocarcinoma	1	78	141[b]
100 mg	Male	52	No	Adenocarcinoma	1	143	141[b]
200 mg	Female	69	No	Adenocarcinoma	1	26	140[b]
300 mg[c]	Male	69	Yes	Adenocarcinoma	2	31	51
300 mg	Female	68	No	Adenocarcinoma	1	28	81[b]
300 mg	Female	55	No	Adenocarcinoma	1	82	141

[a] No, patients who have smoked <100 cigarettes in their lifetime; Yes, patients who have smoked >100 cigarettes in their lifetime.
[b] Censored on the day of last tumor evaluation due to absence of disease progression (response ongoing at data cut-off).
[c] Patient started study treatment with 300 mg and the treatment was stopped 29 d after the start due to QTc prolongation. The patient re-started at a reduced dose level (200 mg) 35 d after the start.
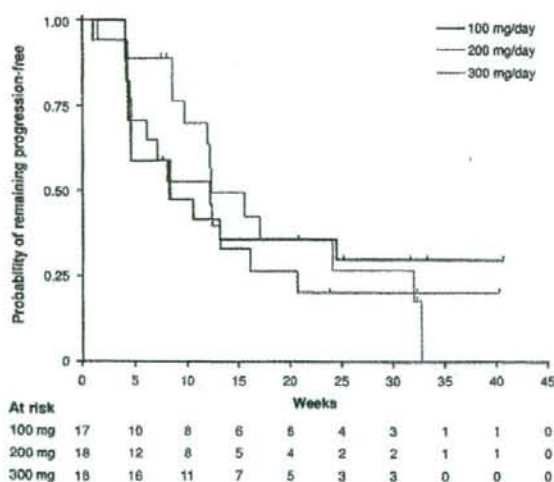
**FIGURE 2.** Kaplan–Meier curve for time to progression.

the common AEs across the three vandetanib arms, although the incidences of diarrhea, constipation, and abnormal hepatic function were numerically higher in the vandetanib 300 mg arm compared with the 100 or 200 mg arms. A dose-dependent increase in the incidence of CTC grade 3 and 4 events was observed; the incidence of these events in the 100, 200, and 300 mg dose arms were 29.4% (5 of 17 patients), 38.9% (7 of 18 patients), and 66.7% (12 of 18 patients), respectively. Of the 24 CTC grade 3 or 4 AEs considered by the investigator to be vandetanib-related, hypertension (100 mg, n = 4; 200 mg, n = 3; 300 mg, n = 3), and asymptomatic QTc prolongation (200 mg, n = 1; 300 mg, n = 1) were reported in more than one patient. Across the three dose levels, the AEs in this study were generally manageable with symptomatic treatment, dose interruption, or reduction.

Six patients discontinued vandetanib because of an AE considered by the investigator to be vandetanib-related: cryptogenic organizing pneumonia (COP), hepatic steatosis, and photosensitivity reaction (each n = 1, 200 mg arm); QTc prolon-

389

TABLE 4. Number of Patients With Most Commonly Reported Adverse Events (Occurring in ≥10% Across all Treatment Groups), Regardless of Causality

MedDRA Preferred Term[a]	Vandetanib 100 mg/d (n = 17)	Vandetanib 200 mg/d (n = 18)	Vandetanib 300 mg/d (n = 18)	Total (n = 53)
Rash (%)	10 (59)	9 (50)	9 (50)	28 (53)
CTC grade 3/4	0/0	1/0	0/0	1/0
Diarrhea (%)	8 (47.1)	8 (44)	11 (61)	27 (51)
CTC grade 3/4	0/0	1/0	1/0	2/0
Hypertension (%)	8 (47)	10 (56)	7 (39)	25 (47)
CTC grade 3/4	4/0	3/0	3/0	10/0
ECG QTc prolonged (%)	4 (24)	9 (50)	8 (44)	21 (40)
CTC grade 3/4	0/0	1/0	1/0	2/0
Photosensitivity reaction (%)	2 (12)	5 (28)	5 (28)	12 (23)
CTC grade 3/4	0/0	0/0	0/0	0/0
Nasopharyngitis (%)	3 (18)	4 (22)	4 (22)	11 (21)
CTC grade 3/4	0/0	0/0	0/0	0/0
Dry skin (%)	2 (12)	4 (22)	5 (28)	11 (21)
CTC grade 3/4	0/0	0/0	0/0	0/0
Nausea (%)	3 (18)	3 (17)	4 (22)	10 (19)
CTC grade 3/4	0/0	0/0	0/0	0/0
Constipation (%)	2 (12)	1 (6)	6 (33)	9 (17)
CTC grade 3/4	0/0	0/0	0/0	0/0
Fatigue (%)	4 (24)	1 (6)	2 (11)	7 (13)
CTC grade 3/4	0/0	0/0	0/0	0/0
ECG QT prolonged (%)	1 (6)	2 (11)	4 (22)	7 (13)
CTC grade 3/4	0/0	0/0	0/0	0/0
Hepatic function abnormal (%)	1 (6)	1 (6)	4 (22)	6 (11)
CTC grade 3/4	0/0	0/0	1/0	1/0
Hematuria (%)	2 (12)	2 (12)	2 (12)	6 (11)
CTC grade 3/4	0/0	0/0	0/0	0/0

[a] MedDRA version 8.1.
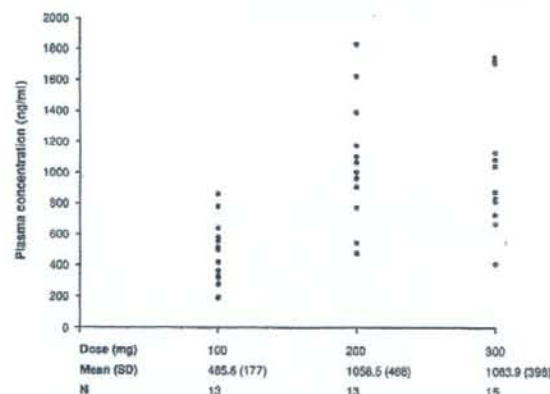
FIGURE 3. Observed maximum vandetanib plasma concentration at day 28. Patients who received dose reduction within the first 28 days were excluded.

Dose (mg)	100	200	300
Mean (SD)	485.6 (177)	1058.5 (466)	1083.9 (398)
N	13	13	15

gation, alanine aminotransferase increased, and erythema multiforme (each n = 1, 300 mg arm). Only COP was classed as a serious AE. Six patients had vandetanib dose reductions due to AEs (100 mg, n = 1; 200 mg, n = 1; 300 mg, n = 4).

Seven patients experienced eight respiratory-related events (COP, dyspnoea, interstitial lung disease [ILD], hypoxia, pneumonitis [all n = 1], and pneumonia [n = 3]). The incidence of these events in the three dose levels was 5.9% (1 of 17 patients; 100 mg), 11.1% (2 of 18 patients; 200 mg) and 22.2% (4 of 18 patients; 300 mg), respectively. Four of these events were considered to be related to vandetanib (COP, ILD, pneumonia [n = 2]). The ILD event was reported in a 64-year-old male patient in the 300 mg arm and resulted in patient death. This event was reported 8 days after vandetanib 300 mg was discontinued because of disease progression. No postmortem examination was performed and the investigator and a third-party physician considered the cause of death to be ILD.

All QTc prolongation was asymptomatic and manageable with dose interruption and/or reduction. The incidence of QTc prolongation was lower in the vandetanib 100 mg (24%) arm compared with the 200 mg (50%) and 300 mg (44%) arms. The mean change in QTc interval from baseline to week 3 (when maximum prolongation was observed) in the 100, 200, and 300 mg arms was +14 milliseconds (range, −25 to 29 milliseconds), +16.5 milliseconds (range, −36 to 49 milliseconds), and +27.6 milliseconds (range, 4 to 51 milliseconds), respectively. Protocol-defined QTc prolongation determined at the treatment site resulted in dose reduc-

come. In contrast, plasma levels of VEGFR-2 showed a trend to decrease over the same period, whereas plasma Tie-2 levels did not seem to change (Table 6). Baseline plasma VEGF levels appeared to be lower in patients who experienced clinical benefit following vandetanib treatment: PR (median 22.3 pg/ml, $n = 6$) and SD (median 37.0 pg/ml, $n = 16$) versus PD (median 63.7 pg/ml, $n = 21$). Patients with a low (below median) baseline plasma VEGF level had a longer TTP (median, 24.1 week) than those with a high (above median) baseline VEGF level (median, 8.3 weeks) (Figure 4). No clear relationship was apparent between baseline levels of plasma Tie-2 and VEGFR-2 and tumor response.

DISCUSSION

The primary objective of this phase IIa study was to assess the ORR to three doses of vandetanib (100, 200, and 300 mg/d) in Japanese patients with advanced or recurrent NSCLC. These doses of vandetanib were selected based on the outcomes of a Japanese phase I study where it was observed that vandetanib was well tolerated up to a dose of 300 mg and objective tumor responses were observed in 4 of 9 patients with NSCLC at doses of either 200 or 300 mg.[11]

In this study, objective tumor responses were observed at all three doses of vandetanib. The ORR in the 100, 200, and 300 mg arms was 17.6% (3 of 17 patients), 5.6% (1 of 18 patients), and 16.7% (3 of 18 patients), respectively. The DCR and TTP were similar across the three dose arms. It was noted that 50% (9 of 18) of the patients in the 200 mg arm had failed two previous chemotherapy regimens, compared with 23.5% (4 of 17 patients) and 22.2% (4 of 18 patients) in the 100 and 300 mg arms, respectively. It is possible that these differences contributed to the lower ORR observed in the 200 mg arm, although the number of patients in each dose arm was too small to allow any definitive conclusions to be made.

Vandetanib was well tolerated at 100, 200, and 300 mg dose levels in this study. Overall, AEs were generally mild

FIGURE 4. Kaplan–Meier curve of low (below median) versus high (above median) baseline plasma VEGF and time to progression.

and manageable with symptomatic treatment, dose interruption or reduction. In addition, the AE profile was consistent with that determined during phase I evaluation in patients with advanced solid tumors[10,11] and phase II monotherapy data in NSCLC.[12] Furthermore, the AE profile was also consistent with that reported previously for agents that inhibit the VEGFR[17,18] or EGFR[4,19] signaling pathways. In general, no apparent dose dependence was noted in the incidence of the common AEs in this study except for asymptomatic QTc prolongation (24%, 56%, and 44% for the 100, 200, and 300 mg dose arms, respectively), an event that was manageable by dose interruption/reduction.
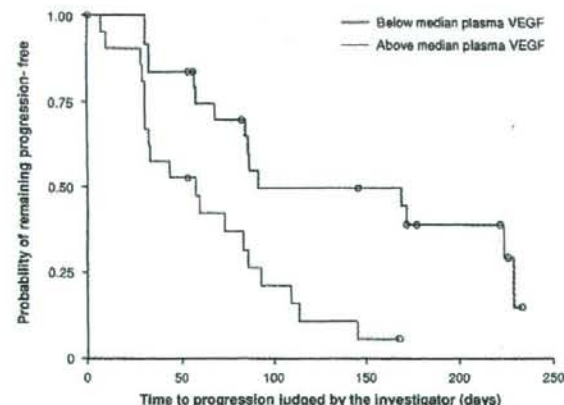
A notable feature of this study, and the phase II program for vandetanib in NSCLC, is that patients with squamous cell histology or stable brain metastases were permitted to enter the trials. Both of these factors have been associated with an increased risk of bleeding, including severe life-threatening hemoptysis in NSCLC patients with squamous histology in a randomized phase II study of bevacizumab with carboplatin and paclitaxel.[20] These events have also been reported with other inhibitors of VEGF/VEGFR signaling, such as sunitinib and sorafenib.[17,18] Importantly, no CNS hemorrhage AEs or hemoptysis attributable to vandetanib were reported in this study.

The PK profile in this NSCLC patient population was consistent with that seen previously during Phase I evaluation in Japanese and USA/Australian patients with a range of solid tumors.[10,11]

In patients with NSCLC, specific *EGFR* mutations are associated with increased sensitivity to EGFR tyrosine kinase inhibitors,[21,22] and a better survival outcome with gefitinib has been shown to correlate with high *EGFR* gene copy number.[23] In this study, an exploratory analysis of tumor samples for amplification of *EGFR* gene copy number and somatic mutations of the *EGFR* gene revealed no clear relationship between *EGFR* mutation or gene amplification status and clinical outcome in patients receiving vandetanib. The *EGFR* mutation frequency of 4% (1 of 27 patients) is lower than that previously reported,[24,25] and further studies are needed to evaluate *EGFR* mutation status as a possible predictive marker for vandetanib therapy in advanced NSCLC.

In addition to *EGFR* mutation/amplification status, plasma profiling of cytokines and angiogenic factors may be a feasible approach for identifying blood-based prognostic and activity markers for therapies in NSCLC. Preliminary analysis of plasma concentrations of the angiogenesis markers VEGF and VEGFR-2 in the present study revealed that patients with PR or SD were more likely to have low baseline levels of VEGF than those with PD. It has been shown previously that low pretreatment levels of circulating VEGF correlated with a good response to gefitinib treatment in patients with NSCLC.[26] The significance of the relationship between these biomarkers and clinical outcome requires further investigation.

In conclusion, vandetanib monotherapy (100–300 mg/d) demonstrated antitumor activity with an acceptable safety and tolerability profile in Japanese patients with advanced NSCLC. Based only on this study, there is no com-

pelling evidence to identify the optimal dose of vandetanib monotherapy in this population of patients; further investigation of vandetanib doses in the range 100 to 300 mg is warranted in Japanese patients with advanced NSCLC. Other randomized phase II studies of vandetanib in advanced NSCLC have demonstrated improvements in progression-free survival with vandetanib 300 mg as a monotherapy versus gefitinib[12] and with the combination of vandetanib 100 mg and docetaxel.[14] Phase III evaluation of vandetanib in a broad population of patients, both as monotherapy at 300 mg (versus placebo in patients previously treated with anti-EGFR therapy [ZEPHYR]; versus erlotinib [ZEST]) and at 100 mg in combination with docetaxel (ZODIAC) or pemetrexed (ZEAL), has been initiated in global trials.

ACKNOWLEDGMENTS

REFERENCES

1. Parkin DM, Bray F, Ferlay J, et al. Global cancer statistics, 2002. *CA Cancer J Clin* 2005;55:74–108.
2. Sandler A, Gray R, Perry MC, et al. Paclitaxel-carboplatin alone or with bevacizumab for non-small-cell lung cancer. *N Engl J Med* 2006;355: 2542–50.
3. Fukuoka M, Yano S, Giaccone G, et al. Multi-institutional randomized phase II trial of gefitinib for previously treated patients with advanced non-small-cell lung cancer. *J Clin Oncol* 2003;21:2237–46.
4. Shepherd FA, Rodrigues PJ, Ciuleanu T, et al. Erlotinib in previously treated non-small-cell lung cancer. *N Engl J Med* 2005;353:123–32.
5. Ciardiello F, Troiani T, Bianco R, et al. Interaction between the epidermal growth factor receptor (EGFR) and the vascular endothelial growth factor (VEGF) pathways: a rational approach for multi-target anticancer therapy. *Ann Oncol* 2006;17:vii109–vii114.
6. Viloria-Petit A, Crombet T, Jothy S, et al. Acquired resistance to the antitumor effect of epidermal growth factor receptor-blocking antibodies in vivo: a role for altered tumor angiogenesis. *Cancer Res* 2001;61: 5090–101.
7. Herbst RS, Johnson DH, Mininberg E, et al. Phase I/II trial evaluating the anti-vascular endothelial growth factor monoclonal antibody bevacizumab in combination with the HER-1/epidermal growth factor receptor tyrosine kinase inhibitor erlotinib for patients with recurrent non-small-cell lung cancer. *J Clin Oncol* 2005;23:2544–55.
8. Wedge SR, Ogilvie DJ, Dukes M, et al. ZD6474 inhibits vascular endothelial growth factor signaling, angiogenesis, and tumor growth following oral administration. *Cancer Res* 2002;62:4645–55.
9. Ichihara M, Murakumo Y, Takahashi M. RET and neuroendocrine tumors. *Cancer Lett* 2004;204:197–211.
10. Holden SN, Eckhardt SG, Basser R, et al. Clinical evaluation of ZD6474, an orally active inhibitor of VEGF and EGFReceptor signaling, in patients with solid, malignant tumors. *Ann Oncol* 2005;16:1391–7.
11. Tamura T, Minami H, Yamada Y, et al. A Phase I dose-escalation study of ZD6474 in Japanese patients with solid, malignant tumors. *J Thorac Oncol* 2006;1:1002–9.
12. Natale RB, Bodkin D, Govindan R, et al. ZD6474 versus gefitinib in patients with advanced NSCLC: Final results from a two-part, double-blind, randomized Phase II trial. *Proc Am Soc Clin Oncol* 2006;abst 7000.
13. Heymach J, Paz-Ares L, de Braud F, et al. Randomized phase II study of vandetanib (VAN) alone or in combination with carboplatin and paclitaxel (CP) as first-line treatment for advanced non-small cell lung cancer (NSCLC). *J Clin Oncol* 2007;25(Suppl 18):abst 7544.
14. Heymach JV, Johnson BE, Prager D, et al. Randomized, placebo-controlled phase II study of vandetanib plus docetaxel in previously treated non small-cell lung cancer. *J Clin Oncol* 2007;25:4270–7.
15. Cappuzzo F, Hirsch FR, Rossi E, et al. Epidermal growth factor receptor gene and protein and gefitinib sensitivity in non-small-cell lung cancer. *J Natl Cancer Inst* 2005;97:643–55.
16. Horiike A, Kimura H, Nishio K, et al. Detection of epidermal growth factor receptor mutation in transbronchial needle aspirates of non-small cell lung cancer. *Chest* 2007;131:1628–34.
17. Gatzemeier U, Blumenschein G, Fosella F, et al. Phase II trial of single-agent sorafenib in patients with advanced non-small cell lung carcinoma. *Proc Am Soc Clin Oncol* 2006;24:abst 7002.
18. Socinski MA, Novello S, Sanchez JM, et al. Efficacy and safety of sunitinib in previously treated, advanced non-small cell lung cancer (NSCLC): Preliminary results of a multicenter phase II trial. *Proc Am Soc Clin Oncol* 2006;24:abst 7001.
19. Thatcher N, Chang A, Parikh P, et al. Gefitinib plus best supportive care in previously treated patients with refractory advanced non-small-cell lung cancer: results from a randomised, placebo-controlled, multicentre study (Iressa Survival Evaluation in Lung Cancer). *Lancet* 2005;366: 1527–37.
20. Johnson DH, Fehrenbacher L, Novotny WF, et al. Randomized phase II trial comparing bevacizumab plus carboplatin and paclitaxel with carboplatin and paclitaxel alone in previously untreated locally advanced or metastatic non-small-cell lung cancer. *J Clin Oncol* 2004;22:2184–91.
21. Lynch TJ, Bell DW, Sordella R, et al. Activating mutations in the epidermal growth factor receptor underlying responsiveness of non-small-cell lung cancer to gefitinib. *N Engl J Med* 2004;350:2129–39.
22. Pao W, Miller V, Zakowski M, et al. EGFReceptor gene mutations are common in lung cancers from "never smokers" and are associated with sensitivity of tumors to gefitinib and erlotinib. *Proc Natl Acad Sci USA* 2004;101:13306–11.
23. Hirsch F, Varella-Garcia M, Cappuzzo F, et al. Combination of EGFR gene copy number and protein expression predicts outcome for advanced non-small-cell lung cancer patients treated with gefitinib. *Ann Oncol* 2007;18:752–60.
24. Paez JG, Janne PA, Lee JC, et al. EGFR mutations in lung cancer: correlation with clinical response to gefitinib therapy. *Science* 2004;304: 1497–500.
25. Janne PA, Engelman JA, Johnson BE. Epidermal growth factor receptor mutations in non-small-cell lung cancer: implications for treatment and tumor biology. *J Clin Oncol* 2005;23:3227–34.
26. Yoshimoto A, Kasahara K, Nishio M, et al. Changes in angiogenic growth factor levels after gefitinib treatment in non-small cell lung cancer. *Jpn J Clin Oncol* 2005;35:233–8.

npg

Mutations in the LKB1 tumour suppressor are frequently detected in tumours from Caucasian but not Asian lung cancer patients

JP Koivunen[1,2], J Kim[3,4], J Lee[3,4], AM Rogers[2], JO Park[1,2], X Zhao[2], K Naoki[2], I Okamoto[5], K Nakagawa[5], BY Yeap[6], M Meyerson[1,2,7,8,9], K-K Wong[1,2,9], WG Richards[10], DJ Sugarbaker[10], BE Johnson[1,2,9] and PA Jänne*[1,2,9]

[1]Lowe Center for Thoracic Oncology, Dana-Farber Cancer Institute, Boston, MA, USA; [2]Department of Medical Oncology, Dana-Farber Cancer Institute, Harvard Medical School, Boston, MA, USA; [3]Department of Thoracic Surgery, Samsung Medical Center, Seoul, Korea; [4]School of Medicine, Sungkyunkwan University, Seoul, Korea; [5]Department of Medical Oncology, School of Medicine, Kinki University, Osaka, Japan; [6]Department of Medicine, Massachusetts General Hospital, Boston, MA, USA; [7]Department of Pathology, Harvard Medical School, Boston, MA, USA; [8]The Broad Institute of MIT and Harvard Universities, Cambridge, MA, USA; [9]Department of Medicine, Brigham and Women's Hospital and Harvard Medical School, Boston, MA, USA; [10]Department of Surgery, Brigham and Women's Hospital, Boston, MA, USA

Somatic mutations of LKB1 tumour suppressor gene have been detected in human cancers including non-small cell lung cancer (NSCLC). The relationship between LKB1 mutations and clinicopathological characteristics and other common oncogene mutations in NSCLC is inadequately described. In this study we evaluated tumour specimens from 310 patients with NSCLC including those with adenocarcinoma, adenosquamous carcinoma, and squamous cell carcinoma histologies. Tumours were obtained from patients of US (n = 143) and Korean (n = 167) origin and screened for LKB1, KRAS, BRAF, and EGFR mutations using RT—PCR-based SURVEYOR-WAVE method followed by Sanger sequencing. We detected mutations in the LKB1 gene in 34 tumours (11%). LKB1 mutation frequency was higher in NSCLC tumours of US origin (17%) compared with 5% in NSCLCs of Korean origin (P = 0.001). They tended to occur more commonly in adenocarcinomas (13%) than in squamous cell carcinomas (5%) (P = 0.066). LKB1 mutations associated with smoking history (P = 0.007) and KRAS mutations (P = 0.042) were almost mutually exclusive with EGFR mutations (P = 0.002). The outcome of stages I and II NSCLC patients treated with surgery alone did not significantly differ based on LKB1 mutation status. Our study provides clinical and molecular characteristics of NSCLC, which harbour LKB1 mutations.
British Journal of Cancer (2008) 99, 245–252. doi:10.1038/sj.bjc.6604469   www.bjcancer.com
Published online 1 July 2008
© 2008 Cancer Research UK

Keywords: carcinoma; non-small cell lung; mutation; LKB1; EGFR; KRAS

Peutz–Jeghers syndrome (PJS) is caused by mutations in the LKB1 tumour suppressor gene (Hemminki et al, 1998). LKB1 is serine–threonine kinase, which has been shown to regulate cell cycle progression, apoptosis, and cell polarity (Tiainen et al, 1999). The major target of LKB1 kinase activity is thought to be AMP-activated protein kinase (AMPK). AMPK is activated under low cellular energy conditions by raising AMP levels and it phosphorylates multiple downstream targets including tubero-sclerosis complex 2 gene, which represses mTOR signalling. Phosphorylation of AMPK by LKB1 is needed for full activity of AMPK and suppression of mTOR activity under low energy conditions (Shaw et al, 2004). The hallmarks of PJS include mucocutaneous pigmentation and hamartomatous polyps of the gastrointestinal tract. Patients with PJS have an increased risk of developing gastrointestinal, pancreatic, breast, gynecological, and non-small cell lung cancers (NSCLC). The overall risk for cancers is increased 5- to 12-fold in different age groups compared with the general population (Hearle et al, 2006). Somatic mutations of the

*Correspondence: Dr PA Jänne, Lowe Center for Thoracic Oncology, Dana-Farber Cancer Institute, D820A, 44 Binney Street, Boston, MA 02115, USA; E-mail: pjanne@partners.org

LKB1 tumour suppressor have rarely been found in cancers from patients who do not have PJS except for NSCLC (Avizienyte et al, 1999). Previous reports have suggested the LKB1 mutation rate to be as high as 30% in NSCLC tumours and cell lines derived from patients of Caucasian origin (Carretero et al, 2004; Matsumoto et al, 2007) and to be infrequent in NSCLC patients of Asian origin (3%) (Onozato et al, 2007). Furthermore, LKB1 mutations have been shown to be associated with adenocarcinoma histology, male gender, and smoking history (Matsumoto et al, 2007). A recent report of using a mouse model for lkb1 inactivation in NSCLC has provided insights into the role of the gene in this cancer. This study showed that lkb1 inactivation in combination with activating mutations of kras using inducible promoters in the lung was associated with decreased survival compared with kras mutation alone (Ji et al, 2007).

Current screening techniques for LKB1 tumour suppressor mutations rely on conventional exonic sequencing of the DNA, which can identify single base pair changes and small deletions/insertions (Ballhausen and Gunther, 2003). The addition of multiple ligation-dependent probe amplification (MLPA), which enables detection of exonic and whole gene deletions, with exonic sequencing has increased the mutation detection rates to 80% in patients with PJS phenotype (Volikos et al, 2006). Conventional

Clinical Studies

246

sequencing has also been used to detect mutations of *LKB1* at mRNA level and some mutations missed by sequencing at the DNA level have been discovered by mRNA-based approaches (Abed *et al*, 2001). However, mutant forms of *LKB1* mRNAs can have a shortened half-life because of nonsense-mediated decay, which can potentially interfere with mutation detection (Abed *et al*, 2001).

We have recently described a rapid and sensitive enzymatic method to detect mutations in epidermal growth factor (*EGFR*) of DNA from fresh tissue and paraffin-embedded tissues (Janne *et al*, 2006). This method includes amplification of region of interest with PCR, SURVEYOR endonuclease digestion of the products, which cleaves mismatched heteroduplex DNAs, and detection of DNA fragments by sensitive high-performance liquid chromatography (HPLC) WAVE HS system. Subsequently, SURVEYOR-positive specimens are fractionated in partially denaturing conditions and are Sanger-sequenced. The major advantages of SURVEYOR-WAVE method are the fast exclusion of wild-type specimens without laborious conventional sequencing and high sensitivity. The SURVEYOR-WAVE method is more sensitive than conventional sequencing as it can detect mutant DNA sequences when they are present in 1% or more of total DNA (Janne *et al*, 2006).

The current study was designed to analyse the incidence of *LKB1* mutations in NSCLC. Furthermore, we wanted to investigate the *LKB1* mutational frequency in different histologies and ethnic backgrounds, and assess their correlation to smoking history, gender, stage, survival, and other oncogenic mutations in NSCLC.

MATERIALS AND METHODS

Cell lines and tumour specimens

The NSCLC cell lines A549, NCI-H1395, NCI-H1650, NCI-H1666, NCI-H1781, NCI-1975, NCI-H23, NCI-H2126, NCI-H441, NCI-H820, HCC2935, HCC4006, and HCC827 were purchased from ATCC (Manassas, VA, USA). H3255, H3255GR, HCC2279, and PC-9 have been previously described (Ono *et al*, 2004; Tracy *et al*, 2004; Engelman *et al*, 2006). Ma1, and Ma70 are NSCLC cell lines harbouring *EGFR* mutations that were established at the Kinki University, Osaka, Japan. A549, NCI-H1395, NCI-H1666, NCI-H23, NCI-H2122, NCI-H2126, and NCI-H460 have previously been reported to contain *LKB1* mutations (Sanchez-Cespedes *et al*, 2002; Bamford *et al*, 2004; Carretero *et al*, 2004).

NSCLC tumours (*n* = 310) were collected from surgical resections from patients with stages I–IV NSCLC when sufficient material for RNA extraction was available. The majority of the specimens (*n* = 167) was collected at the Samsung Medical Center, Seoul, Korea. Frozen tumour tissues were collected from 809 out of 2442 patients who underwent curative resection for NSCLC from November 1995 to February 2007 at Samsung Medical Center. One or two pieces from the periphery of the tumour masses – avoiding necrotic regions – were immediately frozen at −80°C until retrieved. Medical records and haematoxylin and eosin-stained slides of the specimen were reviewed by a single pathologist. Only frozen tumour tissues from adenocarcinoma or squamous cell carcinoma (according to the 2004 World Health Organization histopathological criteria) were included. Only frozen tumour tissues with a tumour cell content of more than 70% were used for further analysis. In addition, frozen tumour tissues of the following patients were excluded from the study: patients who had received preoperative neoadjuvant treatments, patients with double primary lung cancer, and patients who had undergone incomplete resections or who had not been subjected to mediastinal lymph node dissections. Selected frozen tumour tissues were used for the microdissection. Briefly, frozen tissues were lightly stained with haematoxylin–eosin to improve visualisation, and necrotic tumour tissues and intervening normal tissues were removed.

Each of the microdissected tumour tissues with a tumour cell content of more than 90% was placed in 1 ml Easy Blue reagent of a commercially available RNA isolation kit (easy-spin™ Total RNA Extraction Kit, iNtRON Biotechnology, Gyeonggi-do, Korea), immediately homogenised by vortexing, and the total RNA was extracted. The quantity and quality of RNA were analysed using a spectrometer (Nanodrop Technologies, Rockland, DE, USA) and Agilent 2100 Bioanalyzer (Agilent RNA 6000 Nano Kit, Agilent Technologies Inc., Böblingen, Germany), respectively. Finally, 167 frozen tissues with acceptable quality of RNA (RNA Integrity Number (RIN) value over 7.0) were used for the current studies. All patients provided written informed consent.

The tumours from Caucasian patients (*n* = 143) were collected at the Brigham and Women's Hospital, Boston, MA, USA between 1991 and 1997 and have been previously published for patient characteristics and histology, and for expression profile-based clustering of the tumours (Bhattacharjee *et al*, 2001; Hayes *et al*, 2006). Frozen samples of resected lung tumours were obtained within 30 min of resection and subdivided into 100 mg samples and snap frozen at −80°C. Each specimen was associated with an immediately adjacent sample embedded for histology in an optimal cutting temperature medium and stored at −80°C. Six micrometres of frozen sections of embedded samples stained with haematoxylin and eosin were used to confirm the postoperative pathological diagnosis and to estimate the cellular composition of adjacent samples. All specimens underwent pathological review by two pathologists. In all 109 tumours obtained during the same time period were excluded because they did not meet one or more of the eligibility criteria. Tissue samples were homogenised in Trizol (Life Technologies, Gaithersburg, MD, USA) and RNA was extracted and purified by using the RNeasy column purification kit (Qiagen, Chatsworth, CA, USA). Denaturing formaldehyde gel electrophoresis followed by northern blotting using a β-actin probe assessed RNA integrity. Samples were excluded if β-actin was not full length. All patients provided written informed consent. The US cohort included specimens that have previously undergone analyses and the results have been published for *EGFR, KRAS*, and *BRAF* mutations (Bhattacharjee *et al*, 2001; Naoki *et al*, 2002; Hayes *et al*, 2006). We reconfirmed the mutations in 30 of these specimens using the SURVEYOR-based analysis (see section SURVEYOR digestion and HPLC analysis) and found 100% concordance between the two methods (data not shown).

Cell line specimens were snap frozen and stored at −80°C. RNA was extracted from tumours and cell lines using Trizol (Invitrogen, Carlsbad, CA, USA), purified with Rneasy Mini Kit (Qiagen, Valencia, CA, USA) and was used for cDNA synthesis using the QuantiTect reverse transcription kit (Qiagen, Valencia, CA, USA).

PCR primers and cycling conditions

For *LKB1* gene analysis, PCR primers were designed to amplify the cDNA in two amplicons. PCR primers of the first amplicon were designed to hybridise to the noncoding area of the mRNA upstream of exon 1 (5′-agggaagtcggaacacaagg-3′) and to exon 5 (5′-ccagatgtccaccttgaagc-3′) generating a PCR product of 797 bp. The primers for the second amplicon located at exon 5 (5′-aacggcc tggacaccttct-3′) and to noncoding exon 10 (5′-gaaccggcaggaagact gag-3′) generating a product of 702 bp, which has an overlapping part with first amplicon. For SURVEYOR-WAVE analysis of *KRAS*, PCR primers (5′-ggcctgctgaaaatgactga-3′, 5′-tcctgagcctgttttgtgtct-3′) were designed to generate an amplicon of 407 bp covering codons 12, 13 and 61, which are the codons commonly mutated in lung cancers. For SURVEYOR-WAVE mutation analysis of *BRAF*, cDNA was amplified in two overlapping amplicons (5′-aggattt cgtggtgatggag-3′, 5′-gatgacttctggtgccatcc-3′, and 5′-gacgggactcgagt gatgat-3′, 5′-ggtatcctcgtcccaccata-3′) covering codons 387–673. For SURVEYOR-WAVE analysis of *EGFR*, PCR amplification was done in a single amplicon (5′-ggagcctcttacacccagtg-3′,

5′-aggtcatcaactcccaaacg-3′), which covered exons 18–21 of the gene. PCR amplification was done using JumpStart Taq (Sigma, St Louis, MO, USA) under the manufacturer's guidelines. A part of the specimens ($n = 103$) was previously characterised for *KRAS*, *BRAF*, *EGFR* mutations using reverse transcriptase (RT)–PCR and direct sequencing of the PCR products (Naoki *et al*, 2002; Hayes *et al*, 2006).

SURVEYOR digestion and HPLC analysis

SURVEYOR digestion and HPLC analysis were carried out as described previously (Janne *et al*, 2006). In brief, PCR products were digested in reaction mixture containing equal volumes of SURVEYOR enzyme (Transgenomics, Omaha, NE, USA) and Enhancer (Transgenomics, Omaha, NE, USA) at 42°C for 20 min followed by termination of the reaction by Stop Solution (Transgenomics, Omaha, NE, USA). Specimens were then loaded to the WAVE HS HPLC (Transgenomics, Omaha, NE, USA) at 50°C, eluted with an increasing acetonitrile gradient, and detected by UV detector using DNA intercalating fluorescence dye (Transgenomics, Omaha, NE, USA). When cell lines known to be homozygous for specific mutation were analysed, PCR products were mixed 1:1 with PCR products of a wild-type cell line, denatured by heating, and slowly renatured to generate hetero-duplexes.

Sequencing and fractionation

Specimens that showed an altered pattern on the SURVEYOR tracings were purified using QIAquick kit (Qiagen, Valencia, CA, USA) and sequenced bi-directionally by molecular biology core facility of Dana–Farber Cancer Institute. If a specimen showed an altered pattern on the SURVEYOR tracing but had a wild-type sequence by direct DNA sequencing, it underwent fractionation by WAVE HS HPLC in partially denaturing conditions. Running temperatures for specific amplicons were calculated by the Navigator Software (Transgenomics, Omaha, NE, USA). Collected fragments were amplified with PCR using the same primers as in the original amplification, purified and sequenced as previously described above.

Statistical analysis

Fisher's exact test was used to assess the association of *LKB1* mutation status with other clinical, pathological, and genetic characteristics. To adjust for any difference between ethnic groups, the association between *LKB1* mutation rate and each characteristic was also evaluated as stratified contingency tables. If we did not reject that the odds ratios were the same across ethnic groups, we then tested whether the common odds ratios were unity based on the stratified Mantel–Haenszel estimate (Breslow and Day, 1980). Overall survival was estimated using the Kaplan–Meier method, with differences between the groups compared using the log-rank test. All *P*-values were based on a two-sided hypothesis, with $P < 0.05$ considered to be statistically significant and $0.05 < P < 0.10$ considered to be borderline significant.

RESULTS

SURVEYOR-WAVE mutation detection of *LKB1* tumour suppressor in NSCLC cell lines

The impact of the stability of *LKB1* mRNA on detecting *LKB1* mutations was tested using RT–PCR with mRNA extracted from NSCLC cell lines that had previously been characterised for *LKB1* mutations. These included NCI-H441 (wild type) and A549, NCI-H1395, NCI-H23, and NCI-H2126 (all containing *LKB1* mutations). Reverse transcriptase–PCR amplification of the whole coding region of the *LKB1* mRNA showed that cell lines with nonsense (A549, NCI-H23) mutations or 1 bp deletion (H1395) expressed mRNA with comparable size to the wild-type H441 cell line (1460 bp). H2126 cell line, which is known to have homozygous deletion of exons 4–6, expressed mRNA with substantially smaller size (~1000 bp) corresponding to deletion of 398 bp. RT–PCR revealed no major difference in *LKB1* mRNA expression levels between *LKB1* mutant or wild-type cell lines (Figure 1A).

As *LKB1* mutant and wild-type cell lines expressed comparable amounts of *LKB1* mRNA with RT–PCR, we studied the cDNA for mutations using the SURVEYOR-WAVE method. The WAVE HPLC provides a system to analyse DNA fragments smaller than 900 bp and therefore we designed two overlapping amplicons covering exons 1–5 (797 bp) and 5–9 (702 bp) to amplify the whole coding region of *LKB1* mRNA. PCR products of *LKB1* mutant cell lines were mixed 1:1 with the products from wild-type cell lines (H441) to generate heteroduplexes as *LKB1* mutant cell lines were previously reported to be homozygous for the inactivation of the gene. SURVEYOR-WAVE analysis of the amplicon covering exons 1–5 revealed novel peaks with the cDNA for A549, and NCI-H1395 cell lines compared with the wild type from NCI-H441 (Figure 1B). SURVEYOR-WAVE analysis of exons 5–9 showed novel peaks for the NCI-H23 cell line as well. The mutations detected with SURVEOR-WAVE were confirmed by conventional DNA sequencing and they corresponded to previous reports (Sanchez-Cespedes *et al*, 2002; Carretero *et al*, 2004). We could not detect the *LKB1* mutation of H2126 cell line with SURVEYOR-WAVE method using a two-amplicon approach because this cell line has a homozygous deletion of exons 4–6 and the reverse primer of the first amplicon and the forward primer of the second amplicon, which lie on the deleted part of the gene (data not shown).

LKB1 tumour suppressor gene mutations in NSCLC tumours

We next used the SURVEYOR-WAVE method to screen NSCLC tumour specimens ($n = 310$) for *LKB1* mutations. We detected 34 *LKB1* mutations (11%) in the NSCLC tumour specimens (Table 1). The majority of the *LKB1* mutations detected was deletions or insertions ($n = 25$, 74%). The remainder was missense ($n = 7$, 21%) and nonsense ($n = 2$, 6%) mutations (Table 2, Figure 1C). About one-half of the deletions and insertions were small, covering <15 bp ($n = 14$, 56%), whereas larger deletions ($n = 11$, 44%) covering hundreds of base pairs were detected in the remaining specimens. Some mutational hotspots were discovered. The areas that had the same mutation in more than one tumour specimen included deletion of exon 4 ($n = 4$), deletion of exons 2 and 3 ($n = 3$), D194Y ($n = 2$), and P281L ($n = 2$). Interestingly, a significant portion of the mutations was located in exon 1 ($n = 11$, 32%) but there was no area of recurrent mutations in this exon (Table 2). Of the missense mutations detected in the current study, all except R426W are in the kinase domain of the protein. Missense mutations in codons 176 and 194 have been previously characterised in PJS (Launonen, 2005). We also found four F354L alterations (data not shown) but we did not consider these as missense mutations as this alteration has previously been reported to be a rare polymorphism of the gene (Launonen *et al*, 2000). We did not have access to the corresponding normal tissues and therefore, we could not verify if some of the missense mutations were somatic or germline.

Association of *LKB1* tumour suppressor mutations in NSCLC with clinicopathological characteristics

The mutation frequency of *LKB1* gene was significantly higher in NSCLCs in the Caucasian cohort (Table 1). Twenty-five (17% of specimens) of the *LKB1* mutations were detected in NSCLCs
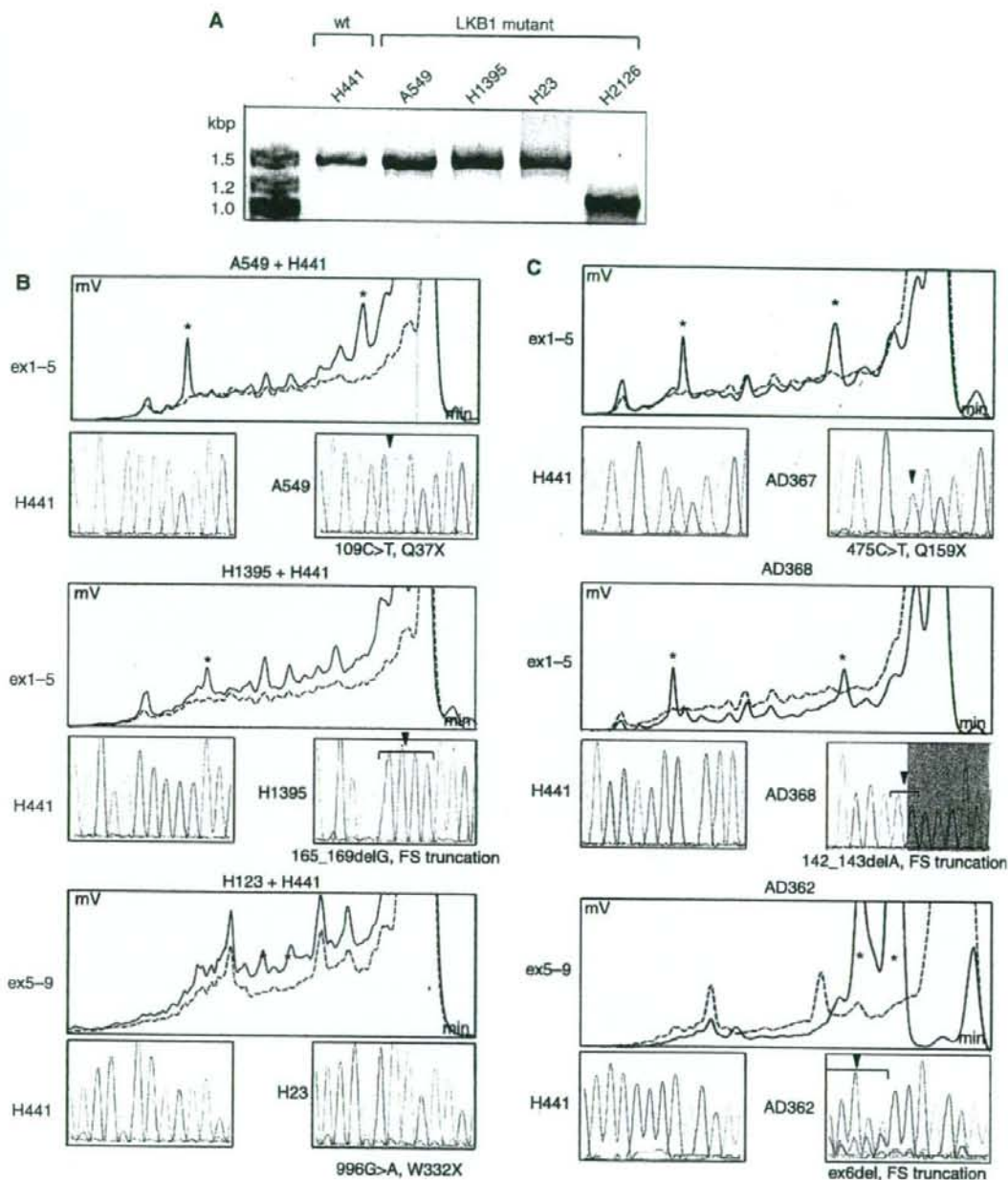
Figure 1 Mutation analysis of *LKB1* gene in NSCLC cell lines and tumours. RT–PCR amplification of cDNA from *LKB1* wt (H441) and *LKB1* mutant (A549, H1395, and H23) cell lines display the full length LKB1 mRNA (1.4 kbp) while the *LKB1* mutant cell line, H2126 with a deletion of exons 4–6 expresses a shorter mRNA (1.0 kbp) (**A**). HPLC tracings of SURVEYOR-WAVE mutation analysis of NSCLC cell lines A549, H1395, or H23 (continuous line), and H441 (dashed line). Time in minutes is shown on the X-axis, voltage in mV on the Y-axis (**B**). A549 and H1395 show novel peaks (*) in the amplicon covering exons 1–5 (ex1–5) corresponding to 109C>T, Q37X and 165_169delG, frameshift and truncation (FS truncation) mutations. The analysis from H23 demonstrates novel peaks in the amplicon covering exons 5–9 (ex5–9) corresponding to 996G>T, W332X mutation. *LKB1* wild-type cDNA (H441) was added to PCR products 1:1, denatured by heating and slowly renaturated to generate heteroduplexes since A549, H1395, and H23 have previously reported to be homozygous for the *LKB1* mutations. SURVEYOR-WAVE mutation analyses of NSCLC tumours (**C**). AD367 and AD368 tumours showed novel peaks in the ex1–5 amplicon corresponding to 475C>T, Q159X, and 142_143delA, FS. truncation mutations. AD362 tumour had novel peaks in ex5–9 amplicon corresponding to deletion of exon 6. Mutant sequences for AD367 and AD368 are displayed from sequences using the forward primer while mutation of the AD362 is showed with reverse primer.

Table 1 Frequency of LKB1 mutations in NSCLC tumours and their association with clinicopathological characteristics

	LKB1 mutation		
	+	−	P-value*
All tumours	34 (11%)	276 (89%)	
Age, median	61.2	62.2	
Ethnicity			
Caucasian cohort	25 (17%)	118 (83%)	0.001
Asian cohort	9 (5%)	158 (95%)	
Gender			
Male	20 (11%)	167 (89%)	NS
Female	14 (12%)	107 (88%)	
Smoking			
Never (<10 py)	2 (3%)	70 (97%)	0.007
Smoker (>10 py)	26 (14%)	161 (86%)	
Tumour stage			
I	19 (10%)	169 (90%)	NS
II	8 (14%)	51 (86%)	
III	5 (11%)	42 (89%)	
IV	1 (12%)	7 (88%)	
Histology			
Adenocarcinoma	27 (13%)	180 (87%)	0.047
Squamous carcinoma	5 (5%)	87 (95%)	
Adenosquamous	2 (22%)	7 (78%)	

*Fisher's exact test, NS = not statistically significant (P > 0.05).

Table 2 The specific LKB1 mutations in NSCLC tumours

Mutation type	No. (%)	Mutation	Amino acid change	Exon	Histology
Missense	7 (21)	ᵃ526G>T	D176Y	4	Ad
		ᵃ580G>T	D194Y	4	Ad
		580G>T	D194Y	4	Sq
		829G>T	D277Y	6	AdSq
		ᵃ842C>T	P281L	6	Ad
		ᵃ842C>T	P281L	6	Ad
		1276C>T	R426W	9	Ad
Nonsense	2 (6)	206C>A	S69X	1	Ad
		475C>T	Q159X	4	Ad
Deletion/ insertion	25 (74)	ᵃ75_76del2&insT	FS, truncates	1	Ad
		120_130del11	FS, truncates	1	Ad
		125_127insGG	FS, truncates	1	Ad
		128_129delC	FS, truncates	1	Ad
		142_143delA	FS, truncates	1	Ad
		180delC	FS, truncates	1	Ad
		209delA	FS, truncates	1	Ad
		227_228delC	FS, truncates	1	Ad
		47_651del604	FS, truncates	1-5	Sq
		153_536del384	FS, truncates	1-4	AdSq
		ᵃexon 2-3del	Truncates	2-3	Sq
		ᵃexon 2-3del	Truncates	2-3	Ad
		exon 2-3del	Truncates	2-3	Ad
		exon 2-4del	FS, truncates	2-4	Sq
		464_465del2insTTTGCT	FS, truncates	3-4	Sq
		562_563delG	FS, truncates	4	Ad
		ᵃexon 4del	FS, truncates	4	Ad
		exon 4del	FS, truncates	4	Ad
		exon 4del	FS, truncates	4	Ad
		exon 4del	FS, truncates	4	Ad
		610_623del14	FS, truncates	5	Ad
		ᵃ837_844delC	FS, truncates	6	Ad
		837_844insC	FS, truncates	6	Ad
		exon 6del	FS, truncates	6	Ad
		1038_1040insG	FS, truncates	8	Ad

Ad = Adenocarcinoma; AdSq = Adenosquamous carcinoma; Sq = Squamous cell carcinoma; . ᵃThese mutations were detected in Korean NSCLC patients.

collected from patients in the United States, whereas only nine mutations (5% of specimens) were detected in the Korean cohort (P = 0.001) (Table 1). The LKB1 mutation rate tended to be higher in adenocarcinomas (13%) compared with squamous cell carcinomas (5%) (P = 0.067). Differences in histological subgroups were relatively modest in the US cohort with mutations in 18 out of 94 (19%) adenocarcinomas vs 5 out of 38 (13%) in squamous cell cancers (P = 0.461). This is in contrast to the findings in the Asian patients where all of the LKB1 mutations were detected in adenocarcinomas (9 out of 113 (8%)) and none were detected in squamous cell cancers (0 out of 54 (0%); P = 0.032). Nevertheless, the higher rate of LKB1 mutation in adenocarcinomas compared with squamous cell carcinomas retains the same level of statistical significance (stratified P = 0.064) after adjusting for fluctuation between ethnic groups. The US cohort also included nine specimens from adenosquamous carcinomas and two out of nine (22%) had LKB1 mutations, which is similar to the frequency in adenocarcinomas in this population (Table 1). There was no association between LKB1 mutations and the clinical stage of the NSCLC patients. Kaplan–Meier survival curves of stages I and II NSCLC patients showed a tendency for shorter survival in patients with LKB1 mutant tumours but this, however, did not reach statistical significance (P = 0.17) (Figure 2). No differences in survival were observed in patients who harboured both LKB1 and KRAS mutations compared with those with KRAS or LKB1 alone but the total number of patients with both mutations who had stages I or II NSCLC was small (n = 9; data not shown). We detected an association of LKB1 mutations with a smoking history (P = 0.007) and only two mutations were detected in tumours from 72 NSCLC patients who were either never or light (⩽10 pack years) former smokers (Table 1). After adjusting for ethnic group, the higher rate of LKB1 mutation among patients with a smoking history is borderline significant (stratified P = 0.067). The reduction in statistical significance is likely owing to the loss of power associated with the overall rarity of LKB1 mutations among never or light former smokers. For these analyses we combined both never

Figure 2 Kaplan–Meyer survival curves of stage I and II NSCLC patients with LKB1 wildtype (red line, n = 198) vs LKB1 mutant (blue line, n = 23) tumours.

smokers and light (⩽10 pack years) smokers as the frequency of mutations in other oncogenes such as EGFR is similar in these two patient groups (Pham et al, 2006). There were no correlations between LKB1 mutations and gender or age of a patient.

Association of LKB1 mutations with K-Ras, B-Raf, and EGFR mutations in NSCLC

Previous reports have suggested that in NSCLC cell lines, LKB1 mutations often occur concurrently with KRAS or BRAF mutations